



1 **Coastal Sources, Sinks and Strong Organic Complexation**
2 **of Dissolved Cobalt within the US North Atlantic**
3 **GEOTRACES Transect GA03**

4

5 **Abigail E. Noble^{1*}, Daniel C. Ohnemus^{1#}, Nicholas J. Hawco¹, Phoebe J. Lam^{1†},**
6 **and Mak A. Saito¹**

7 [1] Woods Hole Oceanographic Institution, Woods Hole, MA, USA

8 [*] now at: Gradient, 20 University Road, Cambridge, MA, USA

9 [#] now at: Bigelow Laboratory for Ocean Sciences, East Boothbay, ME, USA

10 [†] now at: University of California Santa Cruz, Santa Cruz, CA, USA

11 Correspondence to: M. A. Saito (msaito@whoi.edu)

12

13



1 **Abstract**

2 Cobalt is the scarcest of metallic micronutrients and displays a complex biogeochemical
3 cycle. This study examines the distribution, chemical speciation, and biogeochemistry of
4 dissolved cobalt during the U.S. North Atlantic GEOTRACES Transect expeditions
5 (GA03/3_e), which took place in the fall of 2010 and 2011. Two major subsurface sources of
6 cobalt to the North Atlantic were identified by increased abundances of dissolved cobalt
7 relative to surrounding waters. The more prominent of the two was a large plume of cobalt
8 emanating from the African coast off the Eastern Tropical North Atlantic coincident with the
9 oxygen minimum zone (OMZ) likely due to a confluence of processes including reductive
10 dissolution, biouptake and remineralization, and aeolian dust deposition. This occurrence of
11 this plume in an OMZ with oxygen above suboxic levels implies a high threshold for
12 persistence of dissolved cobalt plumes. The other major subsurface source came from Upper
13 Labrador Seawater, which may carry higher cobalt concentrations due to the interaction of
14 this water mass with resuspended sediment at the western margin or from transport even
15 further upstream. Minor sources of cobalt came from dust, coastal surface waters and
16 hydrothermal systems along the mid-Atlantic ridge. The full depth section of cobalt chemical
17 speciation revealed near complete complexation in surface waters, even with the regional high
18 dust deposition. However, labile cobalt was found below the euphotic zone, demonstrating
19 that strong cobalt binding ligands were not present in excess of the total cobalt concentration
20 there and implying mesopelagic labile cobalt was sourced from the remineralization of
21 sinking organic matter. Significant correlations were observed in the upper water column
22 between total cobalt and phosphate, and between labile cobalt and phosphate, demonstrating a
23 strong biological influence on cobalt cycling across much of the North Atlantic transect.
24 Along the western margin off the North American coast, this linear relationship with
25 phosphate was no longer observed and instead a relationship between cobalt and salinity was
26 observed, reflecting the importance of coastal input processes on cobalt distributions. In deep
27 waters, both total and labile cobalt were lower in concentration than at intermediate depths,
28 providing evidence that scavenging may remove labile cobalt from the water column. Total
29 and labile cobalt distributions were also compared to a previously published South Atlantic
30 GEOTRACES-compliant zonal transect (CoFeMUG, GAc01) to discern regional
31 biogeochemical differences. Together, these Atlantic sectional studies highlight the dynamic
32 ecological stoichiometry of total and labile cobalt. As increasing anthropogenic use and



1 subsequent release of cobalt poses the potential to overpower natural cobalt signals in the
2 oceans, it is more important than ever to establish a baseline understanding of cobalt
3 distributions in the ocean.

4

5 **1 Introduction**

6 Cobalt is the scarcest of biologically utilized metals and has a complex marine
7 biogeochemical cycle. The small inventory of oceanic cobalt is maintained by a combination
8 of supply mechanisms, including sedimentary, aeolian, riverine/coastal, and hydrothermal
9 inputs. In particular, the high abundances of cobalt that have been observed as major plumes
10 within the low oxygen waters of major oxygen minimum zones of the South Atlantic and
11 South Pacific (Hawco et al., 2016; Noble et al., 2012), and from more limited datasets from
12 the North Pacific (Ahlgren et al., 2014; Saito et al., 2004; Saito et al., 2005), are likely due to
13 reductive dissolution and advection of sedimentary sources in regions with low-oxygen
14 bottom water sediment-water interfaces (Heggie and Lewis, 1984). Coastal and island sources
15 in oxygenated environments have also been observed, for example, off the North American
16 continental shelf (Saito and Moffett, 2002) and near the Kerguelen Islands (Bown et al.,
17 2012a). While there is limited information regarding the riverine and coastal fluxes of
18 particulate and dissolved cobalt to the oceans, earlier datasets show a significant “desorbable”
19 load of particulate cobalt as well as estuarine sources of organic cobalt complexes (Kharkar et
20 al., 1968; Zhang et al., 1990). The contribution of cobalt from dust has been more difficult to
21 directly observe because of the small amounts of cobalt present in dust relative to iron, with a
22 Co:Fe ratio in crustal material of 1:2600 (equivalent to 30ppm per 3-8% Fe by mass; Taylor
23 and McLennan, 1985), and its likely rapid utilization in the photic zone. Nevertheless,
24 laboratory and field studies have shown evidence for potentially significant dust contributions
25 to upper water column cobalt from anthropogenic and natural dust sources (Shelley et al.,
26 2012b; Thuróczy et al., 2010). While cobalt has been found to be enriched in end-member
27 hydrothermal fluids up to 2570 nM at TAG in the North Atlantic Mid-Atlantic Ridge (Metz
28 and Trefrey, 2000), input is thought to be relatively localized to near-vent environments due
29 to rapid removal by precipitating manganese and iron oxyhydroxides.

30 In addition to these natural sources, there has recently been tremendous growth in the
31 economic market for cobalt through the use of lithium batteries and their cobalt lithium oxide
32 cathode (Scrosati and Garche, 2010). This makes up a relatively new and large mobile



1 reservoir of cobalt throughout the world within electronics, homes, powerplants, cars, and
2 other devices. The environmental impacts of cobalt pollution via mining, smelting, and
3 inappropriate disposal of batteries will likely significantly increase in the future (Banza et al.,
4 2009). A baseline assessment of riverine and oceanic cobalt distributions is critical to inform
5 the development of sustainable economies with regard to trace metal biogeochemical cycles
6 and the future study of the industrial ecology of cobalt.

7 The chemical speciation of cobalt is dynamic in the oceans. Cobalt tends to be strongly bound
8 to organic complexes in the upper water column, but some fraction of dissolved cobalt
9 remains unbound or weakly bound as labile cobalt below the euphotic zone in intermediate
10 and deep waters. In the photic zone and upper water column, saturating concentrations of
11 cobalt binding ligands are often observed, particularly in oligotrophic regimes where
12 cyanobacteria are well represented (Saito and Moffett, 2001; Saito et al., 2005). These ligands
13 are extraordinarily strong, with conditional stability constants on the order of $>10^{16.8}$ (Bown et
14 al., 2012b; Saito et al., 2005), which is significantly higher than those for other transition
15 metals such as iron (FeL_1), for which measured stability constants are on the order of $10^{13.1}$
16 (Rue and Bruland, 1997, Buck et al., 2015). To achieve stability constants in this range, the
17 cobalt-ligand complexes almost certainly have a redox state of Co(III) (Baars and Croot,
18 2015; Saito and Moffett, 2001; Saito et al., 2005), which is consistent with Co(III) being a
19 textbook example of an inert metal redox state (Lippard and Berg, 1994). The structure of
20 cobalt ligands in seawater is currently unknown, but may be related to precursors or
21 degradation products of vitamin B₁₂, a cobalt-containing biomolecule. This complexation by
22 strong organic ligands likely protects and/or slows cobalt from scavenging (Saito and Moffett,
23 2001), as is similarly thought to occur for iron (Johnson et al., 1997). These ligands also have
24 a strong influence on the bioavailability of cobalt to microorganisms (Saito et al., 2002), and
25 the resultant microbial and phytoplankton ecology (Saito and Goepfert, 2008; Saito et al.,
26 2010; Sunda and Huntsman, 1995). While the strongly complexed cobalt is likely somewhat
27 protected from scavenging, the presence of labile cobalt in much of the oceanic water column,
28 should make that fraction particularly vulnerable to scavenging processes. Because
29 complexed and labile cobalt have different physicochemically driven cycles but are inherently
30 linked by biological transformations, cobalt speciation must be considered in efforts to fully
31 understand the biogeochemical cycling of cobalt in the oceans.



1 In recent years, there has been an emergence of ocean studies with high-throughput analyses
2 of dissolved cobalt (Bown et al., 2011; Bown et al., 2012b; Dulaquais et al., 2014a; Dulaquais
3 et al., 2014b; Noble et al., 2012) and labile cobalt (Noble et al., 2012), as a part of the prelude
4 to, or as part of, the international GEOTRACES program (Boyle et al., 2015). These studies
5 have considerably increased the available datasets on dissolved cobalt in the oceans and have
6 contributed to an understanding of cobalt cycling across several diverse biogeochemical
7 regimes. The Benguela Upwelling system appears to be a major source of dissolved Co to the
8 South Atlantic Ocean with a plume extending more than halfway across the basin. Cobalt was
9 also observed to be scavenged more slowly than other hybrid-type metals like Fe and Mn,
10 likely due to its slower oxidation kinetics and lower oxygen abundances in the oxygen
11 minimum zone (Noble et al., 2012). Additional datasets have explored the distribution and
12 speciation of cobalt in the Atlantic and Pacific sectors of the Southern Ocean (Bown et al.,
13 2011; Ellwood, 2008), the Ross Sea and McMurdo Sound of Antarctica (including seasonal
14 variability and under ice early spring conditions)(Noble et al., 2013; Saito et al., 2010), the
15 Eastern Tropical North Pacific and Costa Rica Dome (Ahlgren et al., 2014), the eastern
16 tropical North Atlantic (Baars and Croot, 2015), near the Bermuda, Hawaiian, and Kerguelen
17 Islands (Bown et al., 2012a; Noble et al., 2008; Shelley et al., 2012b), and throughout a
18 meridional transect of the western Atlantic Ocean (Dulaquais et al., 2014a; Dulaquais et al.,
19 2014b). The establishment of these high-throughput sampling and analytical methods for
20 cobalt, largely in response to the GEOTRACES program, has greatly improved our ability to
21 assess and monitor the biogeochemistry of this key micronutrient throughout the global
22 oceans. In fact, before 1990, there were fewer than 200 dissolved cobalt measurements
23 throughout the entirety of the oceans.

24 In this study, we examined the distributions of total dissolved cobalt and labile cobalt in the
25 North Atlantic during the U.S. GEOTRACES North Atlantic Transect (GA03/3_e). The
26 resulting ocean section from this study is compared to the GEOTRACES-compliant zonal
27 section in the South Atlantic Ocean (the CoFeMUG expedition, GAc01; (Noble et al., 2012)).
28 The North Atlantic is an ideal region for the study of biogeochemical processes given the
29 major contributions from aeolian dust deposition from the Sahara desert and Northern
30 hemisphere anthropogenic sources, proximity to coastal and continental sources, strong
31 hydrothermal sources associated with the mid-Atlantic ridge, and recently-formed North
32 Atlantic Deepwater. Moreover, based on previous studies in the South Atlantic, the
33 Mauritanian Upwelling region and the associated oxygen minimum zone were expected to



1 also exert strong influences on the distribution of cobalt in the ocean interior. Two companion
2 manuscripts describe this large dataset: the first describes the methodology, intercalibration
3 and preservation, oceanic distributions, chemical speciation, and major sources of cobalt to
4 the North Atlantic Ocean (Noble et al., this study). The second manuscript examines the
5 ecological stoichiometry of cobalt in zonal transects of the North and South Atlantic Ocean
6 (Saito et al., submitted).

7

8 **2 Methods**

9 Samples were collected along the U.S. GEOTRACES North Atlantic Transect, GA03/3_e
10 chief scientists: William Jenkins, Ed Boyle, and Greg Cutter). This transect was sampled in
11 two legs aboard the R/V Knorr: USGT10 (October 14, 2010 – November 3, 2010; GA03_e)
12 and USGT11 (November 4, 2011 – December 14, 2011; GA03). The first leg (USGT10)
13 departed from Lisbon, Portugal and followed a transect southward, sampling Mediterranean
14 Outflow Water (MOW) and concluding with a short westward transect along 17.4°N, crossing
15 the northern reach of the oxygen minimum zone associated with the Mauritanian Upwelling
16 system. This leg concluded at Station TENATSO at 24.5°W (USGT10-12). The second leg
17 (USGT11) departed from Woods Hole, MA and sampled stations along Line-W to the
18 Bermuda Atlantic Time Series (BATS) Station (USGT11-10, Fig. 1). At an approximately 3°
19 longitudinal spacing, the subsequent stations were sampled across the North Atlantic
20 Subtropical Gyre, including sampling the TAG hydrothermal plume and concluding with a
21 reoccupation of Station TENATSO (USGT11-24).

22 **2.1 Sample Collection**

23 Samples were collected using the Old Dominion University GEOTRACES Carousel on both
24 the 2010 expedition (USGT10) and the 2011 expedition (USGT11). Following the retrieval
25 of the carousel, the pre-conditioned, Teflon-coated Go-Flo bottles were moved to the
26 GEOTRACES Program class-100 trace metal clean van, pressurized with HEPA filtered air,
27 filtered through 0.2 µm Acropak filters in accordance with published methods (Cutter and
28 Bruland, 2012), and immediately refrigerated. Further information regarding deployment of
29 the GEOTRACES carousel can be found on the GEOTRACES website and in the
30 GEOTRACES cookbook (www.GEOTRACES.org). Samples were also collected using the
31 surface towed fish. These samples were collected by suspending the towed fish off the



1 starboard side with a boom, and sampled water at approximately 2m depth using a Teflon
2 diaphragm pump following the GEOTRACES Program Cookbook sampling
3 recommendations.

4 Sample storage bottles were prepared by soaking overnight in the acidic detergent, Citranox,
5 rinsed thoroughly with Milli-Q water (Millipore), filled with 10% HCl to soak for 10 days
6 (Baker Instra-analyzed HCl), rinsed thoroughly with Milli-Q water adjusted to pH 2, and
7 double-bagged, empty. Samples were kept in clean and rinsed 60mL LDPE bottles, and either
8 stored for a short time (<7 days) at 4°C and double-bagged prior to analysis, or for a longer
9 time (6-40 days) at 4°C, double-bagged with gas absorbing satchels and with the outer bag
10 heat-sealed to allow for longer-term sample preservation by removal of oxygen. The gas
11 absorbing satchels were iron-free, obtained from Mitsubishi Gas Chemical (model RP-3K),
12 and each satchel was rated to absorb 60mL of O₂ per 300mL of air. Each heat sealed bag
13 (Ampac™ Flexibles SealPAK Heavy-Duty Pouches, clear polyester 4.5mil) held 6-7 60mL
14 LDPE sample bottles and 3-4 gas absorbing satchels. The satchels come in impermeable,
15 vacuum sealed bags of 25. It would take a few days to use a full bag of 25 satchels, so the
16 bags were expended of air and re-heat-sealed after the required number of satchels were
17 removed in order to limit the exposure of the unused satchels to air. A heat sealer (Kapak by
18 Ampac) was used to seal each bag. After allowing the heat sealer to heat up for 3 minutes,
19 the bags were sealed by lining up the open ends of the bag in the heat sealer and sealing for 1-
20 2 seconds. When samples were ready to be analyzed, the bags were cut open and all samples
21 in the bag were analyzed within a week. Both labile and total dissolved cobalt were analyzed
22 from this sample bottle, and the sample identifier is the allocated GEOTRACES number.

23 **2.2 Total dissolved and labile cobalt analyses**

24 Concentrations of total dissolved and labile cobalt during USGT10 were determined
25 shipboard using a previously described cathodic stripping voltammetry (CSV) method (Saito
26 and Moffett, 2001; Saito et al., 2004). Measurements were made using the Eco-Chemie
27 μAutolabIII systems connected to Metrohm 663 VA Stands equipped with hanging mercury
28 drop electrodes and Teflon sampling cups within 7 days of sampling on double-bagged
29 samples that were kept in the dark at 4°C until analysis. Standard additions of cobalt were
30 carried out with Metrohm 765 Dosimats using a programmed dosing procedure (Noble et al.,
31 2008). Concentrations of total dissolved and labile cobalt from USGT11 were measured on
32 land between 1 and 6 weeks after the sampling date, using the same protocol as that employed



1 for USGT10. Analyses were performed on samples preserved in the dark and in gas
2 impermeable bags with gas absorbing satchels to ensure that no degradation of the sample
3 occurred during that time.

4 For total dissolved cobalt analyses, samples were UV-irradiated for 1 h prior to analysis using
5 a Metrohm 705 UV digester to degrade the organic ligands that bind cobalt and allow binding
6 by the added electroactive cobalt ligand, dimethylglyoxime. Samples were analyzed in 8.5
7 mL aliquots with the addition of 30 μL recrystallized dimethylglyoxime (DMG, Sigma-
8 Aldrich 0.1 mol L^{-1} in methanol), 1.5 mL purified sodium nitrite (Fluka Analytical A.C.S.
9 reagent grade $\geq 99.0\%$, 1.5 mol L^{-1} in Milli-Q water), and 50 μL purified N-(2-
10 hydroxyethyl)piperazine-N-(3-propanesulfonic acid) (EPPS) buffer (Sigma-Aldrich 0.5 mol
11 L $^{-1}$ in Milli-Q water). Reagent purification protocols were modified from those previously
12 published (Saito and Moffett, 2001) in order to accommodate large batches. The DMG was
13 recrystallized after dissolving in an aqueous solution of EDTA to remove any traces of
14 metals. Nitrite solutions were prepared by equilibration overnight on a shaker with Chelex-
15 100 to remove any trace metals. The nitrite solution was then filtered and removed from the
16 chelex, the chelex was rinsed with copious amounts of milli-Q water, and added back to the
17 nitrite solution to equilibrate for a second night on the shaker, followed by filtration into acid-
18 washed HDPE or LDPE bottles. Nitrite was prepared in 500 mL batches and the batches were
19 blank-checked before shipping to sea. Cobalt concentrations were determined by the standard
20 additions technique, with initial concentrations measured in triplicate followed by four 25
21 pmol L^{-1} cobalt additions. A 0.01 mM Co stock solution was prepared by the addition of 14.7
22 μL of a 1000 ppm cobalt standard to a 25 mL Teflon volumetric flask of Milli-Q water
23 adjusted to pH 2. 100 μL batches of 5 nM Co dosing solutions were prepared by the addition
24 of 50 μL of the stock solution to a 100mL HDPE trace metal cleaned volumetric flask of
25 Milli-Q water that was adjusted to pH 3 using Whatman pH indicator paper. This dosing
26 solution was added to the Dosimats and used for the standard additions. Final concentration
27 calculations were adjusted for dilution by the nitrite addition.

28 The analytical blank was determined by analyzing low-trace metal concentration seawater that
29 had been UV-irradiated for 1 h, equilibrated overnight with prepared Chelex 100 resin beads
30 (Bio-Rad), and UV-irradiated a second time to degrade any leached synthetic ligands. This
31 metal free seawater was kept at room temperature in trace metal cleaned Teflon bottles of
32 250ml and 500ml capacity. Blanks for each reagent batch (nitrite, DMG, EPPS) were



1 subtracted from the initial sample concentration. Blank analyses for each reagent batch were
2 made at the beginning and end of use to confirm that the blank remained constant during
3 analyses. The averaged blank for all reagent batches for the entire dataset was $4\text{pM} \pm 1.2$ with
4 a range of 1.7 - 6.3pM ($n = 38$ for individual blank analyses). For a given reagent batch, the
5 standard deviation was smaller, and we report a detection limit (3 times the standard deviation
6 of the blank) of 1.8pM, representing the average of the detection limits estimates for reagent
7 batches with at least 3 blank analyses ($n = 6$).

8 For labile cobalt analyses, 8.5 mL of sample was pipetted into acid washed Teflon vials that
9 were preconditioned with a small aliquot of sample water. 30 μL aliquots of DMG were
10 added to each vial and allowed to equilibrate overnight in the dark prior to analysis (Saito et
11 al., 2004). Analyses were then performed as described for total concentrations using the
12 standard addition technique with the addition of the remaining two reagents immediately
13 before analysis. Previously, we determined that natural cobalt is strongly bound to ligands in
14 seawater with a conditional stability constant of $>10^{16.8}$ (Saito et al., 2005). We define labile
15 cobalt (LCo) as the fraction of total dissolved cobalt (dCo) that is exchangeable with the
16 DMG complexing agent, indicating it is either bound to weak organic/inorganic ligands in
17 seawater or present as free Co(II) (Saito et al., 2004; Saito et al., 2005). Where labile cobalt
18 is detectable, the strong cobalt ligand concentration is defined as the difference between the
19 total dissolved cobalt and the labile cobalt.

20 Two full electrochemical systems were utilized for analyses, with one dedicated to total cobalt
21 analyses and the other to labile cobalt analyses. GEOTRACES standard seawater and internal
22 standard lab seawater were analyzed periodically to ensure that the two electrodes were
23 intercalibrated and functioning properly (Table 1). GEOTRACES standard seawater was UV
24 irradiated and neutralized using 1N Optima ammonium hydroxide to increase the pH to 7.5.
25 An oligotrophic seawater standard internal to our lab (described as CSW for consolidated
26 seawater standard in Table 1), was prepared by UV irradiation in 500mL batches and stored in
27 trace metal clean Teflon bottles at room temperature. The standard was not acidified at any
28 point, thus avoiding the introduction of error and reagent blank associated with adding acid
29 and base (Saito and Moffett, 2002), and allowing regular re-analysis without any further
30 treatment. These standards were used to troubleshoot when the electrodes malfunctioned and
31 to ensure consistency when operational. These batches were measured to be $53 \pm 3 \text{ pM}$ ($n =$
32 4), 74 ± 3 ($n = 9$), $71 \pm 3 \text{ pM}$ ($n = 16$) and $54 \pm 6 \text{ pM}$ ($n = 35$) over the course of the USGT-11



1 cruise analyses, and $53 \pm 5\text{pM}$ ($n = 24$) for the USGT-10 cruise analyses, measured across all
2 reagent batches and both electrode systems. These results demonstrate that the methodologies
3 employed to produce this dataset detect concentrations within the standard deviation of
4 current consensus values for UV-irradiated samples, which can be found on the International
5 GEOTRACES Program website (www.geotraces.org, see below). On occasion analyses were
6 repeated due to obvious electrode malfunction or to confirm oceanographic consistency of
7 measured values. If the repeated measurement was similar to the initial measured value, the
8 initial value is reported. If the repeated analysis was more oceanographically consistent with
9 adjacent values in the water column, that analysis was used instead.

10 **2.3 Intercalibration efforts and data repository**

11 Our laboratory has participated in the GEOTRACES intercalibration effort using this
12 electrochemical analytical technique. We report our laboratory values for the GEOTRACES
13 and SAFe standard analyses using the above-described electrochemical technique, including
14 those conducted during analysis of the US North Atlantic GEOTRACES Section samples to
15 be: SAFe S1 = 5.4 ± 2.6 ($n = 9$), SAFe D2 = 48.3 ± 5.5 ($n=7$), GEOTRACES GS = 31.4 ± 4.1
16 ($n = 24$), GEOTRACES GD = 66.9 ± 6.2 ($n = 30$). These results are in good agreement with
17 those from the GEOTRACES intercalibration effort for Co using different methods all using
18 UV-oxidation to degrade strong cobalt ligands.

19 Comparisons of our CSV data with ICP-MS and flow injection methods at the Bermuda
20 Atlantic Time Series station, a crossover GEOTRACES station, from this expedition and the
21 Dutch GEOTRACES section GA02, generated values that were similar in the photic zone but
22 higher than others' studies in the mesopelagic (Dulaquais Refs). These observations were
23 reported to the GEOTRACES Intercalibration committee and have delayed incorporation of
24 Atlantic dissolved cobalt data into the Intermediate Data Products. The higher mesopelagic
25 values we observed on fresh and "gas-satchel" preserved samples appear to be real based on
26 comparisons with our own unpreserved samples (see Section 3.3 below)

27 All data generated by this lab and discussed in this paper have been submitted to BCO-DMO
28 and are available at <http://www.bco-dmo.org/dataset/3868>. If using this data for future
29 publication or analyses, please cite: Saito, M. (2013) Total dissolved Cobalt and labile Cobalt
30 concentrations from R/V Knorr cruises KN199-04 and KN204-01 in the Subtropical northern
31 Atlantic Ocean from 2010-2011 (U.S. GEOTRACES NAT project). Biological and Chemical



1 Oceanography Data Management Office (BCO-DMO). Dataset version: 2013-04-26. URL:
2 <http://www.bco-dmo.org/dataset/3868>.

3 **3 Results and Discussion**

4 **3.1 Oceanographic Setting**

5 The US GEOTRACES North Atlantic expedition track (Fig. 1) was chosen to investigate
6 multiple processes and provinces within the constraints of an approximately zonal section and
7 was completed in two legs. USGT10 sampled from Portugal to the Cape Verde Islands and
8 consisted of stations USGT10-01 to USGT10-12 (October 2010), and USGT11 sampled from
9 Woods Hole, MA, USA to the Cape Verde Islands, and consisted of stations USGT11-01 to
10 USGT11-24 (November-December 2011). From west to east, the track transited from
11 seasonally productive New England coastal waters, to shelf and slope waters, crossing the
12 deep western boundary current (DWBC) and the Gulf Stream along the repeat hydrography
13 section, Line W. After occupying the Bermuda Atlantic Time Series station (BATS), the track
14 crossed through the oligotrophic Sargasso Sea, the North Atlantic Subtropical Gyre, and the
15 Mid-Atlantic Ridge hydrothermal Trans-Atlantic Geotraverse (TAG) site. From there, the
16 transect continued east, traversing over the northern reach of the tropical North Atlantic
17 Oxygen Minimum Zone near the Cape Verde Islands and Mauritanian Upwelling region off
18 the coast of Northwest Africa. The most eastward samples collected were along a meridional
19 section from Portugal to the Mauritanian Upwelling, and sampled Mediterranean Outflow
20 Water (MOW).

21 **3.2 Vertical Profiles and Sections of Total Dissolved Cobalt and Labile** 22 **Cobalt in the North Atlantic Ocean**

23 The dissolved cobalt data product from USGT10 and USGT11 consisted of 11 and 21
24 profiles, respectively, totalling 717 total dissolved cobalt and 717 labile cobalt data points that
25 were compiled into ocean sections that were rendered with Ocean Data View (Figs 2, 3A-B,
26 Schlitzer, 2011). Visual examination of the vertical profiles (Fig 2) and sections (Fig 3)
27 showed oceanographically consistent results. The two expeditions included a repeat
28 occupation of a station at TENATSO (Tropical Eastern North Atlantic Time-Series
29 Observatory, USGT10-12 and USGT11-24) where the mean difference between the two
30 profiles was 8 pM overall, and 2.2 pM below 2000m. These profiles are expected to be



1 similar given the slow timescale of deeper watermass movement relative to the 1 year
2 sampling interval, and this resampling provides a unique opportunity to examine temporal
3 variability on this time scale throughout the water column. Larger differences were observed
4 in the surface and mesopelagic waters, with little to no difference below 2000m depth. In
5 surface waters, this difference is explained by the fast movement of surface waters and
6 timescales of the processes affecting cobalt cycling in this highly biologically active part of
7 the water column. In mesopelagic waters (particularly between 1500 – 2000m), differences
8 were observed within a water mass characterized as >55% Upper Circumpolar Deepwater
9 (UCPDW) *via* OMPA analysis (Jenkins et al., 2015), indicating some temporal variability at
10 these depths even within the relatively short time scale between samplings.

11 **3.3 Preservation and accuracy of total dissolved cobalt using gas** 12 **absorption satchels**

13 The measurement of total dissolved cobalt has always been a challenge due it having the
14 lowest concentrations of any biologically used metal. During the CoFeMUG expedition slight
15 differences between at-sea analyses and samples returned to the laboratory were observed
16 within the cobalt maximum inside the oxygen minimum zone that raised suspicions of a
17 preservation issue for dissolved cobalt (Noble and Saito, unpubl. data). Moreover, during
18 GEOTRACES intercalibration efforts, two issues have arisen that also contribute to this
19 difficulty in accurate and reproducible total dissolved cobalt measurements. First, during the
20 initial GEOTRACES intercalibration effort, it was confirmed that UV-irradiation was
21 required in all methods to release cobalt from organic ligands that do not degrade or
22 dissociate bound cobalt at low pH. This lack of sensitivity of cobalt ligands to dissociation at
23 low pH is not surprising: it is well known that the cobalt-containing biomolecule vitamin B₁₂
24 survives similarly low pH in the human stomach without dissociation, and that Co(III)
25 complexes are classic examples of kinetic inertness and stability (Lippard and Berg, 1994).
26 As a result, all samples reported as total dissolved cobalt here and in all of our previous
27 studies have been UV-irradiated. More recently, we have become concerned that some
28 intermediate depth samples are prone to loss of dissolved cobalt during storage via redox or
29 other unknown reactions. To document this phenomenon, we present three full profile repeat
30 analyses of USGT10-9 off the coast of Mauritania, analyzed by three preservation protocols:
31 A) at-sea analyses performed within 2 days of sample collection, B) in-lab analyses
32 performed after four months of storage at 4° C in the dark, and C) in-lab analyses of sample



1 duplicates after four months of storage at 4° C in the dark, where the bottles were additionally
2 preserved in air-tight, heat-sealed bags with gas absorbing satchels (Fig. 4). Seawater for the
3 unpreserved, stored analyses (B above) was taken from the same bottles as the at-sea
4 analyses, thus the sample bottles had a large headspace (60 mL bottles with ~50% headspace).
5 These analyses and the at-sea analyses showed similar dissolved cobalt concentrations at the
6 top and base of the water column but showed a large deviation at all other depths (Fig. 4). Use
7 of the gas absorbing satchels to store samples for the same length of time (C above) allowed
8 for excellent recovery of dissolved cobalt with a slope close to the 1:1 coherence of 0.96 and
9 an r^2 of 0.99. Interestingly, almost all of the labile cobalt measured at sea had disappeared in
10 unpreserved samples, indicating the movement of cobalt between chemical forms on the
11 timescale of these experiments (data not shown; Noble and Saito in prep). This has major
12 implications for cobalt speciation on preserved samples in certain biogeochemical regimes,
13 especially the North Atlantic. Interestingly, samples from the Ross Sea did not experience this
14 loss, showing excellent reproducibility on stored, unpreserved samples for both total
15 dissolved and labile cobalt after 17 months (Noble and Saito in prep). However, given the
16 successful recovery of total cobalt demonstrated by this new technique in a region prone to
17 low oxygen and heavy dust inputs, we encourage research groups measuring dissolved cobalt
18 to adopt the preservation method used in this study.

19 A GEOTRACES crossover station was also included at the Bermuda Atlantic Time-Series
20 Station (BATS, USGT11-10). Data were compared between our lab and two labs that relied
21 on an ICP-MS method (Middag *et al.* 2015) at this station as well as at a second station in the
22 North Atlantic Subtropical Gyre (USGT11-20). Our laboratory results were found to be
23 consistently higher than those of the other groups (intercomparison data not shown). The
24 largest discrepancies (~20pM) were observed at intermediate depths associated with the
25 highest labile cobalt concentrations (up to 36pM). Discrepancies were generally smaller in
26 deeper waters (where labile concentrations were often ≤ 10 pM), and concentrations were often
27 within a few pM of each other in the upper few hundred meters where labile concentrations
28 were below 10pM and often below our detection limit. Based on our comparison and
29 preservation experiments in this and other locations, the preservation and storage issue
30 appears to be exacerbated in the North Atlantic, and has only a minor influence at some
31 depths in the South Atlantic, Ross Sea, and South Pacific. Hence, we hypothesize that the
32 preservation effects may be related to the extensive dust- and subsequent colloidal-loading of
33 the North Atlantic region. Ultimately, because comparison of our method with GEOTRACES



1 standards and our internal laboratory standard showed excellent accuracy and reproducibility
2 (see Table 1), we interpret our higher concentrations at intermediate depths to be due to loss
3 of cobalt associated with different preservation techniques used in other methods.. Again, this
4 preservation effect appears to be strongest in the North Atlantic, demonstrating only a minor
5 influence in other regions.

6 **3.4 Major sources of cobalt to the North Atlantic Ocean**

7 The dissolved cobalt data highlight continental margin sources of cobalt to the intermediate
8 waters of the North Atlantic from both eastern and western margins: a large plume emanated
9 from the African coast along the eastern margin (Section 3.4.1), and another large plume was
10 observed along the western margin within Upper Labrador Seawater (ULSW) (Section 3.4.2).
11 In addition, regional contributions from coastal inputs (Section 3.4.3) were observed and a
12 small, localized plume of cobalt was detected above the Mid-Atlantic Ridge hydrothermal
13 vent site at TAG (Section 3.4.5). Atmospheric deposition over the tropical and subtropical
14 North Atlantic is a significant source of a number of metals (e.g. Fe and Mn), but trace cobalt
15 appears to be only a small contribution to the water column inventory. Notably, all elevated
16 source signals of total dissolved cobalt were coincident with elevated labile cobalt as well.
17 While the magnitude of the signals differed between the two species, this elevated signal
18 coincidence may indicate sources carried within a water parcel that experiences slower
19 scavenging relative to surrounding waters (*e.g.* due to low oxygen concentrations) or that the
20 inputs were relatively recent and the maxima were captured in this sampling effort before they
21 were fully scavenged (*e.g.* close to hydrothermal inputs). The following sections discuss these
22 cobalt sources to the North Atlantic Ocean and compare the relative magnitudes of those
23 sources to those observed in a prior study of the South Atlantic Ocean (Noble et al., 2012).

24 **3.4.1 A large plume of cobalt off the Mauritanian Coast**

25 The largest feature of this dataset was the dissolved cobalt plume observed along the eastern
26 margin off of North Africa (Fig. 3). This subsurface plume of dissolved and labile cobalt
27 extended from the Mauritanian coast more than 2000 km into the basin, based on a
28 conservative definition of the plume of exceeding 100 pM total dissolved cobalt (Fig. 3).
29 Centered around the oxygen minimum zone, the highest concentrations of dissolved cobalt
30 (160 pM) were detected at ~400 m depth and were primarily associated with Atlantic
31 Equatorial Waters (AEW). Wind- and circulation-driven upwelling occurs along the



1 Mauritanian coast, leading to higher overall productivity that supports important local
2 fisheries. The subsequent substantial remineralization of organic matter contributes to low
3 oxygen waters at intermediate depths. This Northwest African/Mauritanian Upwelling region
4 contains the smallest of five major marine oxygen minimum zones in the oceans, with the
5 others located in the Eastern Tropical North and South Pacific, the Eastern South Atlantic,
6 and the Arabian Sea (Keeling et al., 2010). Previous cobalt studies have shown that the South
7 Atlantic OMZ and the two Pacific OMZs all harbor high concentrations of cobalt (Ahlgren et
8 al., 2014; Hawco et al., submitted; Noble et al., 2012; Saito et al., 2004; Saito et al., 2005).
9 The current study confirms high cobalt concentrations in the North Atlantic oxygen minimum
10 zone as well, despite this OMZ having higher O₂ concentrations and lacking the substantial
11 suboxic and anoxic waters found in other OMZs.

12 The elevated cobalt observed in the Mauritanian Upwelling is due to a combination of
13 processes: 1) low bottom water oxygen allowing reductively dissolved cobalt to escape from
14 sediments and be transported long distances with minimal removal, and 2) the poorly
15 ventilated shadow zone waters of the OMZ allowing accumulation of cobalt from vertical
16 export of remineralized biogenic and aeolian cobalt. Similar coupling of processes and
17 elevated cobalt were observed in the South Atlantic OMZ on a GEOTRACES-complaint
18 zonal section (GAc01 also known as CoFeMUG, (Noble et al., 2012). These two parallel
19 transects afford a unique opportunity to compare contributions from multiple sources that
20 result in similar large-scale dissolved cobalt features. The biogeochemistries of the two
21 regions are somewhat distinct: the North Atlantic is heavily influenced by aeolian input from
22 the Sahara Desert and North America, and upwelling off the coast of Mauritania is ~1.8 Sv
23 according to ³He measurements (Jenkins et al., 2015). In contrast, the South Atlantic
24 experiences very low overall dust deposition, and upwelling in the Angola dome and
25 Benguela Upwelling has been estimated to be 2.2 Sv (Frame et al., 2014; Skogen, 1999). In
26 the South Atlantic, the cobalt plume was also centered around the oxygen minimum and was
27 coincident with elevated dissolved manganese and iron (Noble *et al.* 2012). Similarly,
28 elevated manganese and iron were observed coincident with the North Atlantic OMZ,
29 suggestive of similar processes influencing these trends (Hatta et al., 2015). In the South
30 Atlantic, we suggested that the high OMZ concentrations of these hybrid metals, and cobalt in
31 particular, were due to a combination of reductive dissolution, upwelling, advection, and
32 remineralization (Noble et al., 2012). Reductive dissolution can be a source of cobalt *via*
33 release of cobalt associated with manganese oxides in sediments along the coast, as we



1 previously suggested for the South Atlantic OMZ system (process #1 above). This process
2 likely contributes to the plume in the North Atlantic; however, the fraction of the cobalt
3 plume supported by aeolian contributions to the vertical export (process #2 above) would be
4 expected to be higher. Moreover, oxygen concentrations in the North Atlantic are not as low
5 as those observed in the South Atlantic, but particulate FeS₂ has been observed in both the
6 sediments and suspended particulate matter near the Mauritanian Upwelling sampling sites
7 (Lam et al., 2012), suggesting that there may be sufficiently low oxygen concentrations along
8 the shelf to allow the escape of reduced cobalt from the sediments without reprecipitation as
9 oxides. Despite higher mesopelagic oxygen concentrations in the North Atlantic, the
10 dissolved cobalt concentrations were also higher here, likely due to a larger contribution from
11 dust sources in the North Atlantic study area (see Section 3.4.4) and/or through less time
12 exposed to scavenging processes within the ocean interior. With the addition of the
13 GA03/3_e section in the North Atlantic, four of the five world's major coastal OMZ regions
14 have now been found to harbour high concentrations of cobalt (Hawco et al., submitted;
15 Noble et al., 2012; Saito et al., 2005). This adds to the growing evidence that oxygen
16 minimum zones and their accompanying coastal regions are important sources of dissolved
17 cobalt to the oceans. Importantly however, for a basin-scale plume to be observed in the
18 North African OMZ region implies that cobalt plume formation and persistence by slowed
19 scavenging has a higher (low) oxygen threshold than other OMZ processes (e.g.
20 denitrification) that require suboxic or anoxic conditions.

21 3.4.2 Advected sedimentary source from Upper Labrador Seawater

22 Strong total dissolved cobalt and labile cobalt plumes were also observed in the western
23 Atlantic along Line W (USGT11-01 to the Bermuda Atlantic Time Series station (BATS,
24 USGT11-10) between 1000-1500m depth, with no accompanying low oxygen signal. Water
25 mass analyses using Optimum Multi-Parameter Analysis (OMPA, Jenkins et al., 2015)
26 constrains the dissolved cobalt feature to be contained within Upper Labrador Sea Water
27 (ULSW). Low silicate concentrations are a differentiating feature of ULSW and can be used
28 to illustrate this by overlaying silicate contours on a Western Margin section of dissolved
29 cobalt (Fig. 5). Two processes, which are not mutually exclusive, may explain the observed
30 feature: 1) advection of a water mass that contains a higher inventory of cobalt than the
31 surrounding waters and/or 2) coastal input of cobalt released from shelf sediments as ULSW
32 comes in contact with the coastal shelf and slope during the transit south. Hatta *et al.* (2015)



1 observed high Fe and Mn on this same GEOTRACES transect within this water mass and
2 invoked release of these metals from sediments into the water column. Previous studies have
3 also invoked continental margin interaction to explain Fe enrichment in Labrador Sea Water
4 at a station further northeast into the Atlantic basin (Laes et al. 2003), and recent data suggests
5 that Arctic waters may contain very elevated concentrations of cobalt (Saito and Noble
6 unpublished data, Bundie and Saito, unpublished data) which could provide a source of high
7 cobalt to the locations of ULSW ventilation.

8 The ULSW cobalt plume appears to be different in composition from that of the eastern
9 margin Mauritanian Upwelling feature. First, the percentage of labile cobalt is higher (35-
10 40%) in the western margin ULSW feature than within the eastern margin Mauritanian
11 Upwelling (20-25%). Higher particulate cobalt is also observed along the western margin
12 (Fig. 3), and could be related to the higher abundance of both dissolved phases, reflecting
13 increased interaction with this phase via shelf inputs and/or scavenging. The transport of
14 labile cobalt to depths below the photic zone may prevent entrainment of labile cobalt into
15 microbial cycling and its transformation to complexed cobalt. This could explain the
16 speciation differences relative to the eastern basin where the plume is shallower and labile
17 cobalt is a smaller fraction of total cobalt. Oxygen concentrations are also much higher in
18 ULSW than within the Mauritanian Upwelling plume, and further demonstrating that low
19 oxygen is not necessarily critical to sustaining subsurface cobalt plumes. Another possible
20 contribution to the western margin plume could come from remineralized cobalt transported
21 within ULSW from its origin to the north. Cyanobacteria are thought to be major contributors
22 to the oceanic cobalt ligand inventory and their virtual absence in polar regions has been
23 invoked to explain the often higher fraction of labile cobalt found in the euphotic zone of
24 those regions (Noble et al., 2013; Saito et al., 2010). It appears that the cold polar-sourced
25 Labrador Sea waters may also carry that imprint of higher labile cobalt. These potential
26 contributions are not mutually exclusive: it is likely that both continental shelf inputs and
27 advected remineralization signals from cooler regions contribute to this high cobalt feature of
28 the North American continental shelf and slope environment.

29 3.4.3 Coastal sources along the North American Margin

30 In the upper 40-60m along the western margin, surface coastal sources dominate cobalt
31 distributions, and an inverse linear relationship with salinity is observed, indicative of a
32 freshwater endmember source (Fig. 6). While biological processes often drive relationships



1 of cobalt with phosphate instead of salinity, including at most of the stations sampled during
2 GA03/3_e (see section 3.7), these Co:PO₄³⁻ correlations (Co:P hereon) were absent in the
3 Line-W region (Fig. 6). Previous work characterized a similar relationship between salinity
4 and cobalt in the North American margin region (Saito and Moffett, 2002), as well as between
5 salinity and other elements such as copper and nickel (Bruland, 1980). In the current study,
6 the relationship with salinity was similar for labile cobalt, supporting a labile source from the
7 coast. This input of cobalt in conjunction with lower salinities implies potential sources from
8 freshwater input such as rivers or groundwater from the coastal Atlantic region.

9 3.4.4 Evaluating Aeolian sources to the North Atlantic

10 The North Atlantic Ocean is strongly influenced by atmospheric dust deposition,
11 which provides an important source of iron and other metals and has been shown to have
12 impacts on regional nitrogen fixation (Moore et al., 2009). The influence of aeolian input
13 from the Sahara Desert increases moving eastward toward the North African margin
14 (Mahowald et al., 2005; Shelley et al., 2012a, Ohnemus and Lam, 2015). The Sahara is an
15 important source of iron and other metals to the North East Atlantic (Measures 1995;
16 Measures et al. 2008, Shelley et al. 2015). The two legs of the GA03/3_e section both
17 occurred during autumn/winter months in successive years (October-December 2010, 2011),
18 coinciding with the period of lower atmospheric deposition to the western Atlantic as
19 measured at Bermuda, where spring is the major period of deposition (Engelstaedter et al.,
20 2006; Jickells et al., 1990). Dust samples collected on-board this North Atlantic section
21 (GA03/3_e) showed aerosol cobalt loadings associated with lithogenic elements such as Ti,
22 Al, and Fe, with minor contributions from other aerosol types (Shelley et al., 2015),
23 suggesting that desert dust sources were more significant than anthropogenic sources during
24 the GA03/3_e expeditions. Lithogenic dust sources are likely a less significant source of
25 cobalt to the North Atlantic Ocean than they are for other metals such as iron and aluminum
26 because cobalt is much less abundant in crustal material (average Co:Fe ratio of ~1:2600,
27 Taylor and McLennan, 1985), resulting in aeolian influences competing with the large coastal
28 cobalt sources described above. In this section, we examine the contribution of dust to
29 dissolved cobalt inventories using cobalt distributions across the basin, correlations with
30 dissolved aluminum in the eastern basin, and estimates of dust flux contributions and relative
31 to upwelling fluxes.



1 Unlike iron or aluminum profiles, which show persistent surface maxima on GA03/3_e,
2 dissolved cobalt profiles within the upper water column of the oligotrophic gyre were
3 consistently nutrient-like (Fig. 2), with surface concentrations of total cobalt as low as 9 pM
4 due to biological uptake (Fig. 7A-B). This was consistent with the low-dust sampling timing
5 and prior observations. Intriguingly, previously published profiles of total dissolved cobalt at
6 BATS station have displayed either nutrient-like or atmospheric deposition surface
7 maximum-type depending on the time of year sampled, the seasonality of dust deposition
8 (atmospheric deposition is highest during late spring/ early summer), and mixed layer depth
9 (Saito and Moffett, 2002; Shelley et al., 2012b). The absence of a surface maxima at BATS
10 during GA03 was consistent with low dust fluxes during fall and winter months, and with the
11 deepening of the mixed layer, which acts to dilute dust-borne cobalt dissolved into shallow
12 mixed layers during summer.

13 Dust deposition to the oligotrophic gyre appeared to have a small impact on the surface cobalt
14 inventory during the low fall/winter dust flux and deep seasonal mixed layer sampled by the
15 GA03 expedition. Aerosol cobalt deposition near Bermuda can be estimated as the product of
16 aerosol cobalt concentrations determined from shipboard bulk aerosol sampling (0.15 pmol m^{-3}
17 3 for BATS and $0.44 \text{ pmol} \pm 0.28 \text{ m}^{-3}$ including 12 surrounding deployments to BATS,"
18 BATS region" hereon (Shelley et al., 2015)) and a typical dry deposition rate of those aerosols
19 ($1000 \text{ m} / \text{d}$ for the Bermuda Atlantic Time-Series crossover station, Duce et al. 1991). This
20 results in a cobalt deposition flux of $0.15 \text{ nmol} / \text{m}^2 / \text{d}$ (BATS) and $0.44 \text{ nmol} / \text{m}^2 / \text{d}$ (BATS
21 region). The solubility of cobalt in Saharan-derived aerosols collected in the Sargasso Sea has
22 been estimated to be 10% during periods of high dust deposition (Shelley et al., 2012a),
23 similar to longer term dissolution experiments on lithogenic-rich aerosols collected in the Red
24 Sea ($17 \pm 7\%$, Mackey et al., 2014). Combining these three facets (flux, solubility and
25 mixed layer depth) with an observed mixed layer depth of 80m observed during GA03, dust
26 dissolution is estimated to add ~ 0.06 (BATS) to 0.17 (BATS region) pM Co per month. This
27 was a relatively low flux compared to the measured mixed layer inventory of 30 pM at BATS
28 during GA03 for this period of low dust deposition and deep mixed layers.

29 We can also consider the conditions of high dust deposition coincident with the seasonally
30 stratified mixed layer to capture the maximum potential dust contributions to the shallow
31 cobalt inventory. Dust deposition and mixed layer depth at BATS tend to experience strong
32 seasonality with similar phasing (low dust coincident with deep mixed layers and high dust



1 deposition with shallow mixed layers). During the summer when dust fluxes are highest,
2 mixed layers can be < 10 m deep (Steinberg *et al.* 2001). Shallow mixed layers intensify the
3 assimilation of metals from atmospheric deposition because the fluxes are diluted over a
4 smaller volume (Jickells 1999). Annual aerosol cobalt fluxes at BATS were calculated to be
5 $944 \text{ nmol Co m}^{-2} \text{ year}^{-1}$ using ^7Be isotopes and data from July 2011 to June 2012 (Kadko *et*
6 *al.*, 2015). Considering the extreme case where 100% of this annual dust deposition is
7 deposited under highly stratified summer conditions (10m mixed layer depth), with an
8 assumed 10% Co solubility results in an estimated 9.4 pM increase per year to the mixed
9 layer cobalt inventory. This is a potentially significant contribution compared to the dissolved
10 cobalt observed during GA03 (9-36 pM). Moreover, solubility increases with seawater
11 exposure time (Mackey *et al.*, 2014), episodic dust loadings of high intensity, and/or an
12 increased anthropogenic component with higher solubility (Thuróczy *et al.*, 2010) could also
13 enhance the fractional magnitude of aeolian sourced dust to the mixed layer. As a result,
14 higher dust deposition and shallower mixed layer depths that occur in the spring and summer
15 at BATS could explain the non-nutrient-like profiles previously observed (Hansell and
16 Carlson, 2001; Saito and Moffett, 2002; Shelley *et al.*, 2012b).

17 Taken together, these results imply that the strong seasonal cycle at the BATS station creates
18 a dichotomy of aeolian influences on the cobalt inventory in mixed layer. As winter time
19 convective overturning homogenizes the upper water column, the spring and summer dust
20 deposition becomes diluted. When applied to a 100m mixed layer, the same annual dust
21 deposition flux decreases to 0.9 pM per year, increasing the dissolved inventory by a few
22 percent overall (2.5-10% of the range described above). As dissolved cobalt concentrations
23 increase with depth, winter mixing also provides a considerable flux of cobalt to the surface
24 from deeper waters (Saito and Moffett, 2002). As a result, atmospheric cobalt deposition is
25 most apparent in the mixed layer cobalt inventories on seasonal timescales in the North
26 Atlantic.

27 Despite the expectation that dust sources of cobalt from the Sahara Desert may have an even
28 stronger influence on eastern margin cobalt inventories, sedimentary sources appear to be
29 dominant. Closer to the Saharan dust sources to the east, increasing surface cobalt
30 concentrations were observed on GA03/3_e (Fig. 7A-B). Previously, surface cobalt
31 concentrations of up to 110 pM (higher than those observed on GA03/3_e) were measured in
32 this region and attributed to dissolution of Saharan aerosols (Bowie *et al.* 2002). Yet, because



1 both dust deposition and coastal upwelling occur in this region, elevated surface
2 concentrations near the eastern margin cannot be solely attributed to dust deposition.
3 Similarly elevated dissolved cobalt was also observed near the coastal margin across the
4 South Atlantic zonal transect, which experiences much lower dust inputs than the North
5 Atlantic (Fig. 7C). Moreover, eastern margin profiles of dissolved cobalt from both
6 expeditions were similar in structure and concentration despite major differences in dust
7 supply and a closer proximity of North Atlantic margin profiles to the coast than those in the
8 South Atlantic, implying that sedimentary sources were dominant in both OMZ regions (Figs.
9 7E-F, see caption).

10 Upwelling can be demonstrated to be the major source of cobalt to the euphotic zone in the
11 North East Atlantic. Similar to the estimates at BATS, the contribution of aerosol dust to
12 dissolved cobalt can be estimated from the aerosol cobalt concentrations measured on
13 GA03/3_e (Shelley et al., 2015), standard deposition velocities (Duce et al., 1991), and
14 relative solubility (Shelley et al., 2012). Dust inventories in North African dominated aerosols
15 along USGT10 averaged $17 \text{ pmol Co m}^{-3}$ (Shelley et al., 2015), over 100-fold higher than that
16 measured at BATS ($0.15 \text{ pmol Co m}^{-3}$, discussed above). These measurements imply a
17 soluble cobalt flux on the order of $1.7 \text{ nmol m}^{-2} \text{ d}^{-1}$ to the mixed layer between USGT10-08
18 and USGT10-12. Due to the elevated cobalt in the OMZ plume described above, upwelling
19 fluxes of dissolved cobalt to the mixed layer are significant here. Jenkins et al. 2015 estimated
20 upwelling rates during GA03/3_e to be 5 m d^{-1} (Jenkins et al., 2015). A dissolved cobalt
21 concentration at the base of the mixed layer of $\sim 50 \text{ pM}$ implies an upward flux 250 nmol m^{-2}
22 d^{-1} . As a result, the soluble cobalt flux from dust during GA03/3_e ($1.7 \text{ nmol m}^{-2} \text{ d}^{-1}$) is only
23 $\sim 1\%$ of the upwelling flux ($250 \text{ nmol m}^{-2} \text{ d}^{-1}$). However, Ohnemus and Lam also observed
24 that the particulate material found in the mesopelagic of this region had a strong lithogenic
25 signal that they attributed to dust fluxes, presumably through sinking dust material (Ohnemus
26 and Lam, 2015), raising the possibility for a gradual dissolution of cobalt from sinking
27 lithogenic particles, as observed experimentally by Mackey et al. (2014). Overall, these flux
28 calculations show that the sub-surface cobalt inventory observed on the eastern portion of this
29 transect buffered the cobalt inventory from dynamic dust deposition, although there may also
30 be a component of dust supply within this subsurface inventory with particle sinking and
31 dissolution.



1 Tracers of dust input can help distinguish external sources of cobalt from dust, and
2 comparisons between dCo:dAl in the North and South Atlantic surface waters show
3 significant differences. Despite the dominance of upwelling fluxes of cobalt in the Eastern
4 North Atlantic, dissolved cobalt was observed to correlate with dissolved aluminum, a tracer
5 of lithogenic dust deposition in surface waters between USGT10-08 and USGT10-12 ($r^2 =$
6 0.96, Fig. 7, dissolved aluminum data from Measures *et al.* (Measures *et al.*, 2015)). The slope
7 of this relationship (1-2 mmol dCo: mol dAl) was much steeper than that expected from their
8 relative abundance in aerosols on GA03/3_e (0.16 mmol Co : mol dAl), despite their similar
9 solubilities in North African aerosols (5-15% Buck *et al.* 2010; Mackey *et al.* 2015; Shelley *et*
10 *al.* 2012b). Perhaps this deviation was related to artifacts in solubility measurements or
11 differential biological processing: productivity is quite high in the Mauritanian Upwelling
12 region and this dCo:dAl relationship in surface waters may reflect rapid uptake of both
13 elements (biological uptake for cobalt and scavenging for aluminum) and subsequent release
14 by remineralization. This influence was evident in depletion of both elements in the upper
15 water column (Figs. 2, 3), and in dAl's lower abundance in the eastern (near Africa) portion
16 of the GA03/3_e transect relative to the west (near BATS, (Measures *et al.*, 2015)).
17 Intriguingly, this dCo:dAl relationship was not observed in surface waters of the Benguela
18 Upwelling where dust input was much lower, but upwelling was also strong (Noble *et al.*,
19 2012). This coupling of dCo and dAl in the North Atlantic implies both an influence of dust
20 and a complex interaction with the high productivity of the upwelling region.

21 As demonstrated above, high cobalt concentrations in the underlying OMZ cause upwelling
22 fluxes of cobalt to be much larger than dust dissolution. Since cobalt in the surface ocean is
23 acquired by phytoplankton, exported to depth and then remineralized, it is possible that
24 atmospheric deposition of cobalt contributes to the OMZ cobalt plume indirectly, thereby
25 returning to the surface ocean when these waters are upwelled. Tritium/helium ages of these
26 water masses have ventilation ages on the order of several decades (Jenkins *et al.* 2015),
27 allowing cobalt originally delivered to the surface ocean to accumulate in the OMZ after it is
28 remineralized. Continued dissolution of cobalt from dusts that have already sunk below the
29 euphotic zone may provide an additional cobalt source to these depths (Mackey *et al.* 2014).
30 Therefore, despite instantaneous dust fluxes that are dwarfed by ocean mixing, storage of
31 dust-derived cobalt in the mesopelagic ocean may cause dust-borne cobalt to be significant in
32 sustaining the cobalt inventory in the North Atlantic Ocean on longer timescales.



1 **3.4.5 Hydrothermal source of cobalt to the deep North Atlantic**

2 The influence of hydrothermalism on dissolved and particulate cobalt was clearly detectable
3 in near-field mid-Atlantic ridge samples, but unlike iron and manganese, these effects did not
4 persist appreciably beyond the ridge station. In the North Atlantic deep water concentrations
5 of cobalt were low (39-55 pM), likely due to scavenging and the intrusion of deep water
6 masses with a smaller cobalt inventory. Samples taken at the TAG hydrothermal field
7 (USGT11-16), however, showed a subtle increase in cobalt concentration relative to the
8 surrounding waters (Fig. 2, 3, 8). Five samples were taken within the plume between 3200
9 and 3500m depth above the well-studied TAG hydrothermal vent site (Fig. 8). A maximum in
10 both dissolved and labile cobalt was observed, constituting a ~37% increase over adjacent
11 depths within the vertical profile for a ~25pM hydrothermal signal over background of which
12 ~16pM is labile cobalt. The presence of labile cobalt in the hydrothermal plume implies that
13 cobalt was released primarily in a labile form and that the vent may act as a local but small
14 source of cobalt to surrounding waters.

15 Cobalt concentrations in hydrothermal vents have previously been studied at TAG and can be
16 taken as potential mixing endmembers (James et al., 1995; Swanner et al., 2014). Suspended
17 particulate cobalt exhibited a dramatic maximum in the hydrothermal plume (12.5 pM pCo,
18 Fig. 8), a 20-fold increase over the background concentrations (~0.6 pM pCo) as observed in
19 the particulate cobalt ocean section (Fig. 3). The differences between the dissolved cobalt and
20 dissolved iron and manganese within the hydrothermal maximum were staggering: iron
21 concentrations reported in the plume are almost 4 orders of magnitude higher than that of
22 cobalt, and manganese concentrations are 3 orders of magnitude higher (Hatta et al., 2015).
23 These iron and manganese features were observed at adjacent stations as well, while the
24 cobalt feature was confined to the near-ridge region at USGT11-16. These large differences
25 should be considered in light of their respective background concentrations away from the
26 vents: Cobalt concentrations are approximately 1 order of magnitude less than that of iron,
27 and approximately 4-fold less than that of manganese. Thus, even taking the higher relative
28 concentrations of iron and manganese into account, the near-field net hydrothermal source
29 difference between metals was major. Dramatically high concentrations of particulate iron
30 oxyhydroxides were also observed at the vent site (~50nM pFe, Ohnemus and Lam, 2015),
31 which likely controlled the overall modest increase in dissolved cobalt distributions by
32 dominating cobalt scavenging. Evidence for localized scavenging at the vents was also



1 observed in negative dCo:P relationships in samples closest to the TAG vent site (see
2 companion manuscript, Saito et al., submitted, their Figs. 6 and 7, bottom depths of station
3 1116). Interestingly, no similarly dramatic increase in pMn was observed, implying the near-
4 field Co scavenging was related to iron oxide precipitation rather than Mn-oxidizing bacterial
5 activity (Ohnemus and Lam, 2015).

6 Cobalt comprises a much smaller fraction of crustal material than these other metals, so
7 hydrothermally leached crust may be expected to reflect similar ratios to that found in crustal
8 material. When dissolved cobalt and iron reported above are normalized to manganese, the
9 relative values are consistent with the dilution of hydrothermal fluids measured at Rainbow,
10 one of the vents located at TAG (Fig. 8, (Hatta et al., 2015; James et al., 1995)). This
11 observation is also consistent with the relative concentrations detected just above the Mid-
12 Atlantic Ridge in the South Atlantic where no notable cobalt feature was found amidst
13 pronounced Mn and Fe plumes (Fig. 8, (Noble et al., 2012; Saito et al., 2013)), likely due to
14 the dilution of the hydrothermal cobalt contributions to below the NADW background
15 inventory. The observation of the hydrothermal cobalt signal in the North Atlantic zonal
16 transect but not the South Atlantic zonal transect was likely a result of the targeted and close
17 sampling of a known hydrothermal field, while the South Atlantic transect accidentally
18 observed a large hydrothermal plume without prior knowledge of any nearby potential
19 hydrothermal field sources to the sampling locations. Circulation patterns at vent sites may
20 also be characterized by circulation patterns that are constrained by the bathymetry of the
21 spreading system, creating a local swirling effect that may allow particle reactive metals to
22 precipitate with less lateral advection (Baker et al. 1995). We also observe an interesting
23 trend among these ratios. Where the ratio of Co:Mn increases with dilution (*i.e.* from direct
24 hydrothermal fluid sampling, to intentional plume sampling around a temperature anomaly, to
25 accidental plume sampling with no observed temperature anomaly), the Fe:Mn ratio follows
26 the opposite trend. Vents from different areas are known to be characterized by different
27 source ratios of metals so this comparison may be coincidental. It is also consistent with what
28 would be expected of the relative differences in biogeochemical oxidative removal rates of
29 these metals, where cobalt tends to be scavenged more slowly than manganese and iron.
30 Additionally, it might also be explained by a difference in the relative importance of
31 hydrothermal vs. other sources of dCo and dMn to their respective deep ocean inventories.



1 **3.4.6 No discernible source of cobalt from Mediterranean Outflow** 2 **Water**

3 Off the coast of Portugal near the opening to the Mediterranean Sea, Mediterranean Outflow
4 Water (MOW) was sampled at Stations USGT10-01 to USGT10-08 within the Meridional
5 section at a depth range of ~1000-1500m (Jenkins et al., 2015)(Figs 2 and 3). There was no
6 discernible MOW source of elevated cobalt to other Atlantic water masses, similar to a lack of
7 dissolved iron in MOW observed on this transect (Hatta et al, 2015). Previous studies have
8 observed slightly elevated concentrations of these metals (Bowie et al., 2002; Morley et al.,
9 1997), and high aluminum concentrations associated with MOW have been used to help trace
10 the presence of MOW (Measures et al., 2015; Measures et al., 1995). This section also
11 revealed slight increases in Pb concentration coincident with MOW (Noble et al. 2015).
12 Significantly elevated lithogenic particle loads were also identified in these samples
13 (Ohnemus and Lam, 2015) though, suggesting perhaps that any labile particulate cobalt may
14 have already been released or otherwise removed from these particles. Cobalt concentrations
15 were quite uniform within MOW during this expedition, which may be reflective of the short
16 residence time of the Mediterranean Sea of ~100 years (Lacombe et al., 1981).

17 **3.5 Variable Influence of Deep Margin Nepheloid Layers**

18 The role of the sediment-water interface and sediment resuspension in nepheloid layers has
19 long been thought to influence the distributions of trace metals, yet few expeditions have
20 sampled these deep regions, and none we are aware of for dissolved cobalt. The North
21 Atlantic zonal GEOTRACES section provided a useful opportunity to examine these potential
22 interactions, and evidence suggests that the differences in cobalt concentration in deep waters
23 along the margins are more complex than dissolution and release near the bottom: the
24 processes that stir up and create nepheloid layers, which provide increased surface areas for
25 scavenging removal of cobalt, can also promote benthic release of dissolved cobalt. Here we
26 observed a variable influence of nepheloid layers on the distributions of dissolved cobalt (not
27 contributing or removing cobalt), that may be related to particle density and composition.

28 Along the western margin of the North Atlantic transect, a pronounced nepheloid layer was
29 sampled at USGT11-06 and USGT11-08 (characterized by suspended particulate mass
30 maxima (SPM) of 763 µg/L at USGT11-08, USGT11-06 was not sampled for particles), and a
31 less dramatic but larger nepheloid layer at USGT11-10 (SPM maximum of 40 µg/L, Lam et



1 al. 2015, Fig. 9). The bottom two depths at USGT11-06 (~4500 – 4900m) showed slightly
2 (~3 pM) elevated total dissolved cobalt relative to the waters above. This could be due to
3 contributions from different water masses that have experienced differing degrees of
4 scavenging over time and/or release of cobalt from the nepheloid layer sampled therein. The
5 bottom two samples are associated with a higher percentage influence of Iceland Scotland
6 Overflow Water (ISOW) relative to the four shallower samples above (~3500 -4300m), which
7 correspond with a higher percentage of Denmark Strait Overflow Water (DSOW, (Jenkins
8 et al., 2015)). These water mass differences are supported by changes in the $^{206}\text{Pb}/^{207}\text{Pb}$
9 isotope signature as well, which gives some indication of the contributions from different
10 water masses due to the isotope signatures captured at their respective outcroppings, both
11 spatially and temporally (Noble et al. 2015). At the BATS crossover station (USGT11-10),
12 several samples were collected near the bottom, and again, a slight increase in labile and total
13 cobalt was observed. A thick nepheloid layer extended several hundreds of meters into the
14 water column but produced a gradual and small decrease in transmittance voltage, unlike the
15 dramatic decrease observed at USGT11-08.

16 It should be noted that transmittance voltage is not the best indicator of suspended particulate
17 mass due to differential sensitivity to particles of different composition. It does give an
18 indication of the presence of these features, which have been confirmed and characterized
19 more quantitatively by chemical determinations of SPM (Lam et al. 2015). The deepest
20 samples show a slight increase in both the total (8pM) and labile (5pM) concentration
21 approaching the deepest sample, possibly suggestive of some resuspended and redissolved
22 particulate cobalt. This slight increase in dissolved cobalt concentration was accompanied by
23 a strong increase in suspended particulate cobalt (Fig. 9). If this increase were due solely to
24 dissolution of resuspended particulate cobalt, a much stronger dissolved cobalt increase may
25 have been expected at USGT11-08. At USGT11-08, however, where the most dramatic
26 decrease in transmittance voltage was observed, and the highest deepwater concentration of
27 suspended particulate cobalt was observed, there was no significant increase or decrease in
28 dissolved total or labile cobalt. No major differences were observed among the water masses
29 occupying the bottom depths between USGT11-06, USGT11-08, and USGT11-10. These
30 contrary observations suggest a balancing act between the source function of resuspension
31 (benthic release of dCo) and the sink function of the nepheloid layer itself (increased surface
32 area for scavenging, i.e. SPM). It is possible that at USGT11-10, the SPM maximum (40
33 $\mu\text{g/L}$) was not high enough to overcome the source from benthic release. At USGT11-08;



1 however, the much higher SPM (763 $\mu\text{g/L}$) may have sufficiently scavenged any cobalt from
2 benthic sources. The composition of the lithogenic particles that dominate these nepheloid
3 layers, are also not particularly good scavengers (Lam et al. 2015), and this composition is
4 likely a key factor driving the differences observed between the western and eastern margins.

5 Along the eastern margin, USGT10-09 also sampled a notable, though smaller,
6 nepheloid layer (SPM max of 44 $\mu\text{g/L}$, Lam et al. 2015), and in this case, a distinct minimum
7 was observed in both total dissolved cobalt and labile cobalt, coincident with a significant
8 maximum in suspended particulate cobalt (Fig. 9). This nepheloid layer, unlike the western
9 margin nepheloid layer, contained particulate manganese and iron oxyhydroxides, which are
10 likely much more efficient scavengers of cobalt than lithogenic particles (Lam et al. 2015).
11 Labile cobalt was undetectable in the deepest sample, suggesting that all cobalt was tightly
12 complexed or that the labile fraction had been scavenged away. This decrease in labile cobalt
13 was also observed at Stations UGST10-10 and USGT10-11, where much smaller nepheloid
14 layers were observed, coincident with relatively small concentrations of resuspended
15 particulate cobalt (Fig. 9). This dramatic difference where some bottom samples along the
16 western margin show slight enrichment while some bottom samples along the eastern margin
17 show strong depletion, both in the presence of notable nepheloid layers and elevated
18 particulate cobalt was intriguing (e.g. compare USGT11-10 to USGT10-09), and
19 demonstrates the chemical diversity of the dissolved and particulate phase interactions. Future
20 characterization of the particle composition in these margin samples and process studies could
21 provide mechanistic explanations for the capacity of particles acting as sources or sinks of
22 cobalt to the dissolved pool.

23 **3.6 Inverse Relationship with Oxygen and Implications for** 24 **Deoxygenation**

25 In intermediate depths, and particularly within the eastern margin cobalt plume, cobalt and
26 dissolved oxygen showed a significant inverse relationship (Fig. 10). As mentioned in
27 Section 3.4.1, elevated concentrations here are likely driven by a combination of a
28 sedimentary source involving reductive dissolution and advection, as well as remineralization
29 of sinking biological material. Both of these processes are linked to oxygen in an inverse
30 fashion and are the likely explanation for this linear relationship. The low O_2 concentrations
31 also allow for the persistence of high dissolved cobalt through slowed oxidation into
32 manganese oxide particles (Moffett and Ho, 1996). In our previous study of the South



1 Atlantic, we discussed the potential for trace metal ocean inventories to increase as a result of
2 ocean deoxygenation (Noble et al., 2012), based on observations compiled by Stramma et al.
3 of deoxygenation within the major oxygen minimum zones across the world oceans over the
4 last 50 years (Stramma et al., 2008). In our South Atlantic work, we made a back-of-the-
5 envelope calculation of the influence of increasing ocean deoxygenation and potential for
6 increasing sedimentary release of cobalt assuming a linear relationship in concert with
7 deoxygenation rates determined by Stramma et al. While this assumption that the linear
8 inverse $d\text{Co}:\text{O}_2$ relationship would be constant moving forward in time is simplistic since its
9 mechanistic basis remains unknown, it provides a useful first approximation of potential
10 increases in cobalt ocean inventories.

11 Here, we apply the same approach to the North Atlantic OMZ to estimate the potential
12 increase in cobalt inventory in the upper 1000m of the North Atlantic that may be attributed to
13 deoxygenation. Within the low oxygen region of the North Atlantic, between 300-800m
14 depth, cobalt and O_2 display an inverse relationship with a slope of $-0.56 \text{ pmol } d\text{Co } \mu\text{mol}^{-1} \text{ O}_2$
15 ($n = 73$, $r^2 = 0.89$), very similar to our findings in the South Atlantic (-0.56 , $r^2 = 0.73$, (Noble
16 et al., 2012)). This suggests that a similar chemistry governs the relationship, not an aspect of
17 a preserved coastal $d\text{Co}:\text{O}_2$ signature, and could be related to the oxygen needs of manganese
18 oxidation and co-oxidation. Stramma et al. estimated an ocean deoxygenation rate for the
19 North Atlantic OMZ of $-0.34 \mu\text{mol } \text{O}_2 \text{ kg}^{-1} \text{ y}^{-1}$ over the past 50 yr (Stramma et al., 2008).
20 Together, these relationships can be used to estimate potential future increases in cobalt
21 concentrations within the oxygen minimum zone. An upper 1000m cobalt inventory from
22 USGT11-10 (BATS) across the basin to the most coastal station at USGT10-09 was estimated
23 by summing the estimated dissolved cobalt within each of many trapezoid shaped water
24 parcels, utilizing each depth and the distance between adjacent stations to interpolate cobalt
25 concentrations between stations and between samples. We then estimated the potential impact
26 of deoxygenation rates on the cobalt inventory within the OMZ, and that subsequent impact
27 on the upper 1000m inventory as a whole by using the $d\text{Co}:\text{O}_2$ relationship and North Atlantic
28 deoxygenation rate described above. The upper 1000m is utilized because of the low O_2
29 waters found in the 250-850m depth range, although this calculation could be easily modified
30 for other depth ranges. Extrapolating forward 100 years, using this simple calculation we
31 estimate that the cobalt inventory in the upper 1000m of the North Atlantic could increase by
32 20% in the next 100 years. These large potential changes in upper ocean inventories may have
33 implications for the ecological balance within this basin. This increase is also two-fold higher



1 than the ~10% estimated for the South Atlantic, which is largely due to the two-fold higher
2 rate of deoxygenation reported for the North Atlantic OMZ ($-0.34 \mu\text{mol O}_2 \text{ kg}^{-1} \text{ y}^{-1}$) relative to
3 the South Atlantic OMZ ($-0.17 \mu\text{mol O}_2 \text{ kg}^{-1} \text{ y}^{-1}$, (Stramma et al., 2008)). These results imply
4 a need to consider the influence of changing oceanic oxygen on the biogeochemistries of
5 metals and their influence on marine ecology.

6 **3.7 Relationships of dissolved and labile cobalt with soluble reactive** 7 **phosphate in the upper Atlantic Ocean**

8 Dissolved cobalt distributions in the oceanic upper water column are influenced by biological
9 processes such as uptake and remineralization (Noble et al., 2008). The nutrient stoichiometry
10 of the aggregate microbial ecosystem can be inferred using a similar approach to that
11 originally used by Alfred Redfield for dissolved and particulate nitrogen and phosphate
12 (Redfield et al., 1963), where linear relationships between dissolved cobalt and soluble
13 reactive phosphate can be interpreted as time-integrated signals of the extent of cobalt
14 utilization by the resident phytoplankton community and their subsequent remineralization
15 from the biological particulate phase. The aggregate slope of this correlation is termed the
16 “ecological stoichiometry” for their inferred biological usage (Sterner and Elser, 2002). An
17 emerging distinguishing feature of cobalt relative to other macro (N and P) and micronutrients
18 (Zn and Cd) is a much larger range in stoichiometries when different oceanic regions are
19 compared (Noble et al., 2012; Noble et al., 2008; Saito et al., 2010) (Baars and Croot, 2015;
20 Bown et al., 2011; Sunda and Huntsman, 1995). The production of large GEOTRACES
21 datasets provides an opportunity to explore this variability in stoichiometry and the processes
22 behind them. Here, we describe broad regional differences in the Co:P relationships in the
23 North Atlantic. A detailed and finer-scale analysis of these relationships and their ecological
24 interpretations are discussed in a companion manuscript (Saito et al. in prep).

25 When the North and South Atlantic zonal datasets (NAZT and CoFeMUG) were compared in
26 an aggregate scatter plot (Fig. 10), there were two notable differences. First, there is a shift
27 toward lower phosphate concentrations relative to cobalt concentrations in the North Atlantic
28 when compared to the South Atlantic. This is likely due to the lower surface phosphate
29 inventory observed in the North Atlantic relative to the South Atlantic (Noble et al., 2012; Wu
30 et al., 2000), as was evident in comparisons of nitrate+nitrite versus phosphate on these two
31 transects and the higher phosphate axis intercept in the South Atlantic (Fig 10A). Second,
32 there was also an offset in cobalt abundances, with higher total dissolved cobalt in the North



1 Atlantic that consistently approached ~150pM in the eastern North Atlantic (Fig. 2), likely
2 due to the higher atmospheric cobalt flux and resultant concentrations in the North Atlantic
3 relative to the South Atlantic. As mentioned earlier, the North Atlantic experiences significant
4 aeolian input from the Saharan Desert compared to the much lower dust inputs to the South
5 Atlantic (Noble et al., 2012), and aeolian deposition is not considered to be a major source of
6 phosphorus. This offset can also be seen in the dCo:O₂ plot as a vertical shift (Fig. 10), also
7 likely caused by the higher dust contribution in the North Atlantic and an overall greater
8 inventory.

9 Dissolved labile cobalt (LCo) also showed linear relationships with phosphate in the North
10 Atlantic (Fig. 11), where labile cobalt is defined as the sum of the free cobalt and the cobalt
11 bound to weak ligands (Saito et al., 2004). To our knowledge, this is the first report of linear
12 relationships between labile cobalt and phosphate. Unlike the frequent observations of excess
13 strong iron binding ligands in oceanic photic zones (Buck, 2007; Buck et al., 2015; Rue and
14 Bruland, 1997), strong cobalt binding ligand concentrations tend to be less than or equal to
15 total Co, allowing frequent detection of labile cobalt in the water column, and the potential for
16 large swings in bioavailability of cobalt. The coherent lower slope of the LCo:P relative to
17 total cobalt in the water column below the upper photic zone is particularly intriguing as it
18 contrasts an apparent steeper and less coherent LCo:P in the upper photic zone. The low
19 labile cobalt in the upper photic zone was expected due to phytoplankton and microbial
20 uptake, reflective of the scarcity of this labile cobalt form and resulting in it comprising a
21 small fraction of total dissolved cobalt there. The correlation labile cobalt with phosphate in
22 the ocean interior (Fig. 11) implicates a remineralization source from decaying phytoplankton
23 material. It is possible that cobalt taken up by phytoplankton and prokaryotic microbes for use
24 in enzymes or vitamin B₁₂ is present in a proteinacious form intracellularly that is susceptible
25 to degradation with proteolytic activity upon sinking and results in its release as labile cobalt.
26 This would be in contrast to strongly complexed cobalt that is formed through insertion into
27 corrin rings of the B₁₂ precursor by cobaltochelatase enzymes (Bonnet et al., 2010; Rodionov
28 et al., 2003; Saito et al., 2005). This duality in cobalt's chemical forms, having both
29 complexed and labile forms, adds a layer of variability in availability and geochemical
30 cycling that is similar to that of dissolved and colloidal size fractions of iron (Bergquist et al.,
31 2007; Fitzsimmons and Boyle, 2014). This fraction of the labile cobalt is likely a less
32 protected inventory relative to scavenging processes and even though it is a small component
33 of the dissolved cobalt inventory, it could play a major role in cobalt biogeochemical cycling.



1 **3.7.1 Variation in the depth of the cobaltclines: evidence for** 2 **dynamic biogeochemistry**

3 Examination of individual vertical profiles, with a focus on several stations from USGT10,
4 further reveals the dynamic nature of cobalt chemical speciation and its influence on cobalt
5 biogeochemical cycling in the photic zone of the North Atlantic (Fig. 12). With the exception
6 of the labile cobalt at station USGT10-06, dissolved cobalt, labile cobalt and phosphate are all
7 drawn down to their lowest concentrations in the mixed layer. By comparing these species to
8 biological and physical proxies such as fluorescence and density, a few subtle differences
9 emerge that are influenced by changes in the mixed layer depth and chlorophyll max. At all 4
10 stations, the gradient in total cobalt concentrations, or the “total cobalt-cline” coincides with
11 the base of the mixed layer. At USGT10-09, the “phosphocline” and the “labile cobalt-cline”
12 also coincide with the base of the mixed layer. Here, the waters are particularly productive as
13 seen by the intensity of the fluorescence peak, and the three analytes reach relatively high
14 concentrations due to upwelling, potential aerosol inputs (3.4.4), and sedimentary sources
15 from the plume as discussed earlier (3.4.1). The chlorophyll maximum was shallow and
16 pressed up against the base of the mixed layer as a result of the upwelling.

17 We can compare this to the patterns observed at USGT10-03, where less productivity was
18 observed due to a lack of significant external nutrient sources and correspondingly smaller
19 local sub-mixed layer nutrient inventories (note the scale difference). Here, the total
20 cobaltcline again coincides with the mixed layer depth (77 m), but phosphate and labile cobalt
21 are both drawn down below detection, much deeper, into the middle of the chlorophyll
22 maximum (99m, Fig. 12, (Shelley et al., 2012a)). In the other two stations as well, the
23 chlorophyll maximum is smaller and deeper, and the labile cobaltcline follows the
24 phosphocline, where the total cobaltcline remains coincident with the mixed layer depth,
25 revealing a confluence of processes that are occurring on relatively short timescales. With a
26 short residence time of 0.32 y in the upper water column (upper 100m; Saito and Moffett,
27 2002), the tug of war between biochemical and geochemical processes within one profile can
28 be seen. This offset between the labile and total cobaltclines suggests that biological processes
29 act quickly enough to complex labile cobalt that enters the chlorophyll maximum at a rate
30 faster than upward mixing. While pigment samples from this transect were lost during freezer
31 failure, making assessment of the biological contributions to these variations difficult, we
32 know that generally the coastal regions of the Atlantic have more eukaryotic phytoplankton



1 representation, while the oceanic regions are dominated by picocyanobacteria and
2 picoeukaryotes (Olson et al., 1990), and that picocyanobacteria are sources of metal binding
3 ligands in both open ocean and coastal waters, including for cobalt and copper (Moffett and
4 Brand, 1997; Saito et al., 2005). In the Mauritanian Upwelling, the inventories are higher and
5 productivity is more intense, but the chlorophyll maximum is pressed up against the mixed
6 layer so the differences in rates of uptake, complexation, diffusion, mixing, and upwelling
7 cannot be easily separated.

8 **3.7.2 Loss of cobalt from intermediate and deep waters by** 9 **scavenging**

10 In addition to the variety of sources that contribute cobalt to the North Atlantic
11 described above, there is evidence for a dissolved sink from the pelagic water column
12 throughout this North Atlantic zonal transect. This is evident in the vertical structure of
13 profiles that, unlike nutrient-like elements such as phosphate and zinc, decrease precipitously
14 at intermediate depths: below ~1000m in the western and northeastern Atlantic profiles and
15 below ~600m on the eastern profiles off of Mauritania (Fig. 2). These changes in vertical
16 structure likely reflect a shift in the balance between long-term scavenging removal processes
17 occurring on horizontally advecting water masses relative to the vertical input of dissolved
18 cobalt from remineralizing sinking particles. These scavenging processes can be observed in
19 aggregate through an examination of the relationship between total dissolved cobalt and
20 soluble reactive phosphorus (dCo:P) across the basin that displayed a downward curl,
21 reflective of a loss of total dissolved cobalt relative to phosphate consistent with a preferential
22 scavenging of total dissolved cobalt (Fig. 13), likely into bacterially-formed manganese oxide
23 particles (Lee and Tebo, 1994; Moffett and Ho, 1996). Examination of the water masses
24 calculated through OMPA analysis (Jenkins et al., 2015) associated with datapoints in dCo:P
25 space showed water masses with unique signatures. In particular, the combined deep DSOW-
26 AABW-ISOW (~ >3000m depth, Denmark Strait Overflow, Antarctic Bottom Water, and
27 Iceland-Scotland Overflow) and CLSW (~2000-3000m, Classical Labrador Seawater) water
28 masses were the major contributors to the North Atlantic scavenged “curl” feature (Fig 13C)
29 implying loss of cobalt relative to phosphate in those water masses during their long-term
30 advection. This cobalt curl feature is also evident in the South Atlantic zonal section as well,
31 largely overlapping with the features observed here (Fig. 13A and 13B). Finally the amount of
32 dissolved cobalt at intermediate depths decreases from the North Atlantic to the South



1 Atlantic, consistent with a scavenging loss with thermohaline circulation. The accompanying
2 manuscript (Saito et al. submitted) conducts further statistical analysis and discussion of the
3 scavenging process through a profile-by-profile examination of the dCo:P relationship.

4 Notably there were also instances where regional circulation influences the otherwise
5 generally “typical” hybrid-type profile structure. For example, vertical structure was notably
6 perturbed at station USGT10-07 where sharp concentration gradients appear coincident with
7 jetting intrusions of water masses as indicated by oxygen concentration, water mass analysis
8 (Jenkins et al., 2015), and SF₆ tracer age (Smethie et al. in prep) (Fig. 14).

9 **4 Conclusions**

10 The dissolved and labile cobalt datasets for the North Atlantic zonal transect reveal numerous
11 sources of cobalt to the North Atlantic. A large plume of cobalt was observed at ~400 m depth
12 within the Mauritanian Upwelling along the eastern margin, which reflect eastern margin
13 dissolved cobalt sources that are concentrated in the OMZ by phytoplankton uptake, export
14 and remineralization and dust inputs. The western margin also displayed an elevated cobalt
15 feature at intermediate depths characterized by ULSW, likely due to the mobilization of
16 cobalt from continental shelf sediments either before or after subduction of the ULSW
17 watermass. Hydrothermal and aeolian sources were detectable but small relative to these
18 larger ocean features. Variable sources and sinks of cobalt were observed in deep margin
19 nepheloid layers, suggesting that particle composition and sediment redox gradients may play
20 an important role and should be taken into consideration in future studies. Using
21 deoxygenation rates and a relationship between cobalt and O₂, we estimate that the cobalt
22 inventory in the upper 1000m of the North Atlantic may increase by 20% in the next 100
23 years due to ocean deoxygenation, approximately twice that previously estimated for the
24 South Atlantic OMZ region. Differences in the ecological stoichiometry of cobalt observed in
25 the upper water column imply that a wide variety of cobalt utilization regimes exist. The
26 processes of uptake and remineralization exerted control on cobalt in the oligotrophic surface
27 waters of the North Atlantic, demonstrated by correlations with phosphate, and the strong
28 drawdown of phosphate, nitrate, and total dissolved and labile cobalt. When low salinity,
29 coastal, metal inputs and physical processes imposed a strong influence along Line-W, these
30 correlations were obscured, muting the influence of biological processes that operate to
31 couple these species. Combining growing datasets of cobalt coming from the GEOTRACES



1 program with future biochemical studies will improve our understanding of the influence of
2 cobalt biogeochemical cycling and its interaction with ocean marine ecology.

3 Increasing anthropogenic cobalt use due to growth in the economic market for cobalt in
4 lithium batteries and other sources poses the potential to drastically change global oceanic
5 cobalt distributions since the potential environmental impact of cobalt pollution is currently
6 unknown. As such, it is more important than ever to establish a baseline understanding of
7 cobalt distributions in the ocean to provide important insight into its oceanic biogeochemical
8 cycling and to inform potential future impact of industrial use of cobalt on the ocean
9 inventory.

10

11 **Author contribution**

12 At-sea and laboratory analyses of total dissolved and labile cobalt were conducted by A.
13 Noble. Data analysis and manuscript writing were conducted by A. Noble, M. Saito, and N.
14 Hawco. Particulate sample collection, analyses, and interpretations in the text were
15 conducted by P.J. Lam and D. Ohnemus.

16

17 **Acknowledgements**

18 We would like to thank the GEOTRACES Expedition Team, including the Chief Scientists
19 Ed Boyle, Bill Jenkins, and Greg Cutter, and the GEOTRACES sampling team. We also
20 thank the Captain and Crew of the R/V *Knorr* for their outstanding support of science. We
21 also gratefully acknowledge support of funding agencies on the following grants: the US
22 National Science Foundation (NSF-OCE 0928414, 1233261, 1435056) and the Gordon Betty
23 Moore Foundation (Grant 3738).

24

25

26

27

28

29



1 **Figure Captions**

2 **Figure 1.** Map of USGT10 and USGT11 expedition tracks.

3 **Figure 2.** Dissolved profiles of total and labile cobalt for USGT10 and USGT11. Several
4 stations of note are discussed more fully in the text, but some of note include USGT11-10
5 (BATS), USGT11-16 (TAG), USGT10-09 (Station closest to the Mauritanian coast),
6 USGT11-1 to USGT11-08 (Stations along Line-W). USGT10 was sampled during the fall of
7 2010, and USGT11 was sampled during the fall of 2011.

8 **Figure 3.** (A) Full depth section of total cobalt, (B) full depth section of labile cobalt, and (C)
9 full depth section of particulate cobalt with the meridional section in the right panels and the
10 zonal section in left panels. These ocean sections were created using Ocean Data View. The
11 dissolved sections were created using VG gridding and extrapolated lengths of less than 70
12 permille in either y or x direction for any of the section representations.

13 **Figure 4.** Examination of storage effects and use of gas absorbing satchels for preservation on
14 a vertical profile from Station USGT10-9 collected near Mauritania. “Preserved” samples
15 were kept refrigerated in heat-sealed bags with gas absorbing satchels, while “4 months”
16 samples were only kept refrigerated. The preserved samples showed excellent recovery after
17 four months in cold storage compared with at-sea measurements, while non-preserved
18 samples showed significant loss of dissolved cobalt.

19 **Figure 5.** Section of dissolved cobalt and dissolved silicate along the western margin of the
20 North Atlantic (Line-W). Upper Labrador Sea Water, identified generally between 700 and
21 1500 m depth by OMPA analysis (Jenkins et al., 2015) carries elevated concentrations of
22 cobalt and is depleted in silicate. Elevated cobalt concentrations may be due to interaction of
23 this water mass with sediments along the wide coastal shelf.

24 **Figure 6.** Total and labile cobalt show strong correlations with phosphate in the North
25 Atlantic Subtropical Gyre, but this relationship is not observed along Line-W. Along Line-W,
26 strong relationships between (A, B) salinity and total cobalt and (A, C) salinity and labile
27 cobalt were observed in surface waters.

28 **Figure 7.** Surface transects for (A-B) the north Atlantic zonal section USGT10 and USGT11
29 (top panels), and (C) the South Atlantic zonal section CoFeMUG (Noble et al., 2012). (D)
30 Relationships between dCo:dAl and correlations for northeast Atlantic stations USGT10-08 to
31 USGT10-12. (E-F) Comparison of vertical profiles of dCo between the North and South
32 Atlantic zonal sections near the African Coast. Distances of stations to the African coastline



1 were ~530km for Tenatso (USGT11-24) and 210 km from USGT10-09 in the North Atlantic,
2 and 1300 km for Station 13 and 790 km for Station 15 from the CoFeMUG Expedition in the
3 South Atlantic.

4 **Figure 8.** (A) Manganese-normalized cobalt and iron concentrations in hydrothermal fluid
5 and above the Mid-Atlantic Ridge. Hydrothermally leached crust may reflect ratios of
6 reducible metals that are similar to that found in crustal material. Normalized cobalt and iron
7 values are consistent with what might be expected by dilution of hydrothermal fluids
8 measured at TAG. This is consistent with dissolved data from above the Mid-Atlantic Ridge
9 at 9 ° S as well. The ratio of Co:Mn also increases with presumed dilution (from vent fluids
10 to TAG to 9 ° S), while the Fe:Mn ratio decreases. This is consistent with the expected
11 relative oxidative removal rates of these metals: Co < Mn < Fe. (B) Profiles of dissolved total
12 and labile cobalt above the TAG hydrothermal vent and above the Mid-Atlantic Ridge at 9 °
13 S. A slight maximum in total and labile cobalt suggests that hydrothermally released cobalt at
14 TAG is primarily labile and that the vent may provide a small, local source of cobalt. (C)
15 Particulate cobalt profile at TAG. The dramatic signal of pCo is notable against the
16 background concentrations, but small relative to those observed for Fe and Mn (see text).

17 **Figure 9.** Along the margins, nepheloid layers have differing effects on the dissolved cobalt
18 concentration and composition, suggesting that more complex processes than simple
19 dissolution from resuspended particles. Thick and large nepheloid layers along the western
20 margin (three profiles to the left) appear to have small or insignificant effects on the dissolved
21 and labile cobalt profiles, while a moderate nepheloid layer along the eastern margin at
22 USGT10-09 (profile furthest to the right) appears to have a strong scavenging effect on
23 the dissolved and particularly the labile cobalt. Labile cobalt in the deepest samples here
24 were drawn down below the detection limit. The dramatic differences in the effect of
25 nepheloid layers on the dissolved and labile cobalt concentrations demonstrates great
26 chemical diversity in the dissolved-particulate phase interactions and suggests that
27 these interactions cannot be generalized by phase alone.

28 **Figure 10.** Aggregate nutrient stoichiometries between the North Atlantic and the South
29 Atlantic studies. Basin offsets were observed in comparisons between (A) nitrate and
30 phosphate (linear regression for South Atlantic with a slope of 17.4, r^2 of 0.995) and (B)
31 cobalt and phosphate concentrations in the upper water column of the North and South
32 Atlantic zonal sections (North Atlantic stations, 2-400 m, linear regression depths include 54-



1 300 m, with a slope of 61.4, r^2 of 0.90; S. Atlantic stations 1-19, 54-300m, same depths for
2 linear regression, slope of 52.6, and r^2 of 0.83). (C) Different slopes and intercepts are
3 observed across many regions of the world oceans that have been studied in the literature
4 (Martin et al., 1989; Noble et al., 2012; Saito et al., 2010). These differences arise from
5 variability in cobalt and phosphate utilization and supply. (D) Linear relationships occur
6 between cobalt and oxygen for USGT10, USGT11, and for previous work done in the South
7 Atlantic.

8 **Figure 11.** Co:P ecological stoichiometry observed across different regions in the North
9 Atlantic. A tighter correlation is observed where labile cobalt becomes detectable and the
10 correlation is observed down to differing depths depending on the strength of the processes
11 that affect cobalt and phosphate biogeochemical cycling. Processes that affect both species
12 similarly in time and space will tend to tighten the correlation and deepen the depth to which
13 it is observed (e.g. USGT10-01- USGT10-06). Where scavenging or reductive dissolution
14 may influence the two species differently, the correlation may be more diffuse or not
15 observed at all (CoFeMUG Sta. 8-17).

16 **Figure 12.** In the upper water column, labile cobalt is often drawn down above and within the
17 chlorophyll maximum, following the phosphocline. The total cobaltcline appears to be more
18 closely associated with mixed layer depth. Comparing the differences among the stations that
19 do and do not experience upwelling, it is apparent that biological processes are capable
20 of complexing labile cobalt at a rate faster than upward mixing. This is seen by
21 comparing USGT10-03 (located in oligotrophic waters north of the
22 Mauritanian Upwelling) to stations USGT10-12 (located within the Mauritanian Upwelling).
23 At both locations, the labile cobalt is drawn down below detection into the chlorophyll
24 maximum. Station USGT10-03 is located in oligotrophic waters, with a smaller deep
25 inventory of cobalt (~50pM at the chlorophyll max, increasing to ~60 at 200m). Station
26 USGT10-12, however, is located in waters that experience upwelling and have a much larger
27 deep inventory of cobalt (~70pM at the chlorophyll max, increasing to ~100pM at 200m).

28 **Figure 13.** Full depth relationships of total dissolved cobalt, phosphate, and AOU. In a
29 comparison with water mass analysis from the NAZT expeditions, clear populations of data
30 by water mass origin were observed in both (A) dCo:P and (B) dCo:AOU space. Data from
31 the Ross Sea is also shown as a potential endmember (Saito et al., 2010). dCo:P relationships
32 and the “cobalt curl” deviance from them were observed in the (C) Western and (D) Eastern



1 basins of the Atlantic, and were similar between the North and South Atlantic (South Atlantic
2 data from Noble et al., 2012).

3 **Figure 14.** Intermediate depth profile for (A) O₂, (B) labile cobalt (C) total cobalt (D) SF₆
4 age and (E) water mass as a percent for USGT10-07. A strong linear correlation with O₂ is
5 observed (inset). A small but distinct maximum is observed between 400-600m and
6 demonstrates the capability of water mass features to influence the cobalt vertical profile at
7 these depths.

8



1 **References**

2

3 Ahlgren, N. A., Noble, A., Patton, A. P., Roache-Johnson, K., Jackson, L., Robinson, D.,
4 McKay, C., Moore, L. R., Saito, M. A., and Rocap, G.: The unique trace metal and mixed
5 layer conditions of the Costa Rica upwelling dome support a distinct and dense community of
6 *Synechococcus*, *Limnol. Oceanogr.*, 59, 2166-2184, 2014.

7 Baars, O. and Croot, P. L.: Dissolved cobalt speciation and reactivity in the eastern tropical
8 North Atlantic, *Marine Chemistry*, 173, 310-319, 2015.

9 Baker ET, German CR, Elderfield H. Hydrothermal plumes over spreading-center axes:
10 Global distributions and geological inferences. *Seafloor hydrothermal systems: Physical,*
11 *chemical, biological, and geological interactions.* 1995:47-71.

12 Banza, C. L. N., Nawrot, T. S., Haufrroid, V., Decrée, S., De Putter, T., Smolders, E., Kabyla,
13 B. I., Luboya, O. N., Ilunga, A. N., Mutombo, A. M., and Nemery, B.: High human exposure
14 to cobalt and other metals in Katanga, a mining area of the Democratic Republic of Congo,
15 *Environmental Research*, 109, 745-752, 2009.

16 Bergquist, B., Wu, J., and Boyle, E.: Variability in oceanic dissolved iron is dominated by the
17 colloidal fraction, *Geochimica et Cosmochimica Acta*, 71, 2960-2974, 2007.

18 Bonnet, S., Webb, E. A., Panzeca, C., Karl, D. M., Capone, D. G., and SA, S.-W.: Vitamin
19 B12 excretion by cultures of the marine cyanobacteria *Crocospaera* and *Synechococcus*,
20 *Limnol. Oceanogr.*, 55, 1959-1964, 2010.

21 Bowie, A. R., Whitworth, D. J., Achterberg, E. P., R.Fauzi, Mantoura, C., and Worsfold, P. J.:
22 Biogeochemistry of Fe and other trace elements (Al, Co, Ni) in the upper Atlantic Ocean,
23 *Deep Sea Res. I*, 49, 605-636, 2002.

24 Bown, J., Boye, M., Baker, A., Duviellbourg, E., Lacan, F., Le Moigne, F., Planchon, F.,
25 Speich, S., and Nelson, D. M.: The biogeochemical cycle of dissolved cobalt in the Atlantic
26 and the Southern Ocean south off the coast of South Africa, *Marine Chemistry*, 126, 193-206,
27 2011.

28 Bown, J., Boye, M., Laan, P., Bowie, A., Park, Y.-H., Jeandel, C., and Nelson, D. M.: Imprint
29 of a dissolved cobalt basaltic source on the Kerguelen Plateau, *Biogeosciences*, 9, 5279-5290,
30 2012a.

31 Bown, J., Boye, M., and Nelson, D. M.: New insights on the role of organic speciation in the
32 biogeochemical cycle of dissolved cobalt in the southeastern Atlantic and the Southern
33 Ocean, *Biogeosciences*, 9, 2719-2736, 2012b.

34 Boyle, E. A., Anderson, R. F., Cutter, G. A., Fine, R., Jenkins, W. J., and Saito, M.:
35 Introduction to the US GEOTRACES North Atlantic Transect (GA-03): USGT10 and
36 USGT11 cruises, *Deep Sea Research Part II: Topical Studies in Oceanography*, 116, 1-5,
37 2015.

38 Bruland, K. W.: Oceanographic distributions of cadmium, zinc, nickel and copper in the
39 North Pacific, *Earth Planet. Sci. Lett.*, 47, 176-198, 1980.

40 Buck, C. S., Landing, W. M., and Resing, J. A.: Particle size and aerosol iron solubility: A
41 high-resolution analysis of Atlantic aerosols, *Marine Chemistry*, 120, 14-24, 2010.



- 1 Buck, K. N.: The physicochemical speciation of dissolved iron in the Bering Sea, Alaska,
2 *Limnol. Oceanogr.*, 52, 1800, 2007.
- 3 Buck, K. N., Sohst, B., and Sedwick, P. N.: The organic complexation of dissolved iron along
4 the U.S. GEOTRACES (GA03) North Atlantic Section, *Deep Sea Research Part II: Topical*
5 *Studies in Oceanography*, 116, 152-165, 2015.
- 6 Cutter, G. A. and Bruland, K. W.: Rapid and noncontaminating sampling system for trace
7 elements in global ocean surveys, *Limnology and Oceanography: Methods*, 10, 425-436,
8 2012.
- 9 Duce, R. A., Liss, P. S., Merrill, J. T., Atlas, E. L., Buat-Menard, P., Hicks, B. B., Miller, J.
10 M., Prospero, J. M., Arimoto, R., Church, T. M., Ellis, W., Galloway, J. M., Hansen, L.,
11 Jickells, T. D., Knap, A. H., Reinhardt, K. H., Schneider, B., Soudine, A., Tokos, J. J.,
12 Tsunogai, S., Wollast, R., and Zhou, M.: The Atmospheric Input of Trace Species to the
13 World Ocean, *Global Biogeochemical Cycles*, 5, 193-259, 1991.
- 14 Dulaquais, G., Boye, M., Middag, R., Owens, S., Puigcorbe, V., Buesseler, K., Masqué, P.,
15 Baar, H. J., and Carton, X.: Contrasting biogeochemical cycles of cobalt in the surface
16 western Atlantic Ocean, *Global Biogeochemical Cycles*, 28, 1387-1412, 2014a.
- 17 Dulaquais, G., Boye, M., Rijkenberg, M., and Carton, X.: Physical and remineralization
18 processes govern the cobalt distribution in the deep western Atlantic Ocean, *Biogeosciences*,
19 11, 1561-1580, 2014b.
- 20 Ellwood, M. J.: Wintertime trace metal (Zn, Cu, Ni, Cd, Pb and Co) and nutrient
21 distributions in the Subantarctic Zone between 40–52°S; 155–160°E, *Mar. Chem.*, 112,
22 107-117, 2008.
- 23 Engelstaedter, S., Tegen, I., and Washington, R.: North African dust emissions and transport,
24 *Earth-Science Reviews*, 79, 73-100, 2006.
- 25 Fitzsimmons, J. N. and Boyle, E. A.: Both soluble and colloidal iron phases control dissolved
26 iron variability in the tropical North Atlantic Ocean, *Geochimica et Cosmochimica Acta*, 125,
27 539-550, 2014.
- 28 Frame, C., Deal, E., Nevison, C., and Casciotti, K.: N₂O production in the eastern South
29 Atlantic: Analysis of N₂O stable isotopic and concentration data, *Global Biogeochem.*
30 *Cycles*, 28, 1262-1278, 2014.
- 31 Hansell, D. A. and Carlson, C. A.: Biogeochemistry of total organic carbon and nitrogen in
32 the Sargasso Sea: control by convective overturn, *Deep Sea Research Part II: Topical Studies*
33 *in Oceanography*, 48, 1649-1667, 2001.
- 34 Hatta, M., Measures, C. I., Wu, J., Roshan, S., Fitzsimmons, J. N., Sedwick, P., and Morton,
35 P.: An overview of dissolved Fe and Mn distributions during the 2010–2011 U.S.
36 GEOTRACES north Atlantic cruises: GEOTRACES GA03, *Deep Sea Research Part II:*
37 *Topical Studies in Oceanography*, 116, 117-129, 2015.
- 38 Hawco, N. J., Ohnemus, D. C., Resing, J. A., Twining, B. S., and Saito, M. A.: A cobalt
39 plume in the oxygen minimum zone of the Eastern Tropical South Pacific, *Biogeosciences*
40 Discussion, submitted.
- 41 Heggie, D. and Lewis, T.: Cobalt in pore waters of marine sediments, *Nature*, 311, 453-455,
42 1984.



- 1 James, R. H., Elderfield, H., and Palmer, M. R.: The chemistry of hydrothermal fluids from
2 the Broken Spur site, 29°N Mid-Atlantic ridge, *Geochim. Cosmochim. Acta*, 59, 651-659,
3 1995.
- 4 Jenkins, W. J., Smethie Jr, W. M., Boyle, E. A., and Cutter, G. A.: Water mass analysis for
5 the U.S. GEOTRACES (GA03) North Atlantic sections, *Deep Sea Research Part II: Topical
6 Studies in Oceanography*, 116, 6-20, 2015.
- 7 Jickells, T. D., Deuser, W. G., and Belostock, R. A.: Temporal Variations in the
8 Concentrations of some Particulate Elements in the Surface of the Sargasso Sea and their
9 Relationship to Deep-Sea Fluxes, *Marine Chemistry*, 29, 203-219, 1990.
- 10 Jickells, T. D.: The inputs of dust derived elements to the Sargasso Sea: a synthesis, *Marine
11 Chemistry*, 68, 5-14, 1999.
- 12 Johnson, K. S., Gordon, R. M., and Coale, K. H.: What controls dissolved iron in the world
13 ocean?, *Mar. Chem.*, 57, 137-161, 1997.
- 14 Kadko, D. and Johns, W.: Inferring upwelling rates in the equatorial Atlantic using 7 Be
15 measurements in the upper ocean, *Deep Sea Research Part I: Oceanographic Research Papers*,
16 58, 647-657, 2011.
- 17 Keeling, R. F., Körtzinger, A., and Gruber, N.: Ocean deoxygenation in a warming world,
18 *Annual Review of Marine Science*, 2, 199-229, 2010.
- 19 Kharkar, D. P., Turekian, K. K., and Bertine, K. K.: Stream supply of dissolved silver,
20 molybdenum, antimony, selenium, chromium, cobalt, rubidium and cesium to the oceans,
21 *Geochimica et Cosmochimica Acta*, 32, 285-298, 1968.
- 22 Lacombe, H., Gascard, J., Gonella, J., and Bethoux, J.: Response of the Mediterranean to the
23 water and energy fluxes across its surface, on seasonal and interannual scales, *Oceanologica
24 Acta*, 4, 247-255, 1981.
- 25 Laës A, Blain S, Laan P, Achterberg EP, Sarthou G, De Baar HJ. Deep dissolved iron profiles
26 in the eastern North Atlantic in relation to water masses. *Geophysical Research Letters*. 2003
27 Sep 1;30(17).
- 28 Lam PJ, Ohnemus DC, Marcus MA. The speciation of marine particulate iron adjacent to
29 active and passive continental margins. *Geochimica et Cosmochimica Acta*. 2012 Mar
30 1;80:108-24.
- 31 Lam PJ, Ohnemus DC, Auro ME. Size-fractionated major particle composition and
32 concentrations from the US GEOTRACES north Atlantic zonal transect. *Deep Sea Research
33 Part II: Topical Studies in Oceanography*. 2015 Jun 30;116:303-20.
- 34 Lee, Y. and Tebo, B.: Cobalt(II) Oxidation by the Marine Manganese(II)-Oxidizing *Bacillus*
35 sp. Strain SG-1, *Applied and Environmental Microbiology*, 60, 2949-2957, 1994.
- 36 Lippard, S. J. and Berg, J. M.: *Principles in Bioinorganic Chemistry*, University Science
37 Books, Mill Valley, CA, 1994.
- 38 Mackey, K. R. M., Chien, C.-T., Post, A. F., Saito, M. A., and Paytan, A.: Rapid and gradual
39 modes of aerosol trace metal dissolution in seawater, *Frontiers in Microbiology*, 5, 794, 2014.
- 40 Mahowald, N. M., Baker, A. R., Bergametti, G., Brooks, N., Duce, R. A., Jickells, T. D.,
41 Kubilay, N., Prospero, J. M., and Tegen, I.: Atmospheric global dust cycle and iron inputs to
42 the ocean, *Global Biogeochemical Cycles*, 19, 2005.



- 1 Martin, J. H., Gordon, R. M., Fitzwater, S., and Broenkow, W. W.: VERTEX:
2 phytoplankton/iron studies in the Gulf of Alaska., *Deep-Sea Res.*, 36, 649-680, 1989.
- 3 Measures, C., Hatta, M., Fitzsimmons, J., and Morton, P.: Dissolved Al in the zonal N
4 Atlantic section of the US GEOTRACES 2010/2011 cruises and the importance of
5 hydrothermal inputs, *Deep Sea Research Part II: Topical Studies in Oceanography*, 116, 176-
6 186, 2015.
- 7 Measures, C. I., Yuan, J., and Resing, J. A.: Determination of iron in seawater by flow
8 injection analysis using in-line preconcentration and spectrophotometric detection, *Mar.*
9 *Chem.*, 50, 3-12, 1995.
- 10 Measures CI, Landing WM, Brown MT, Buck CS. High-resolution Al and Fe data from the
11 Atlantic Ocean CLIVAR-CO2 Repeat Hydrography A16N transect: Extensive linkages
12 between atmospheric dust and upper ocean geochemistry. *Global Biogeochemical Cycles*.
13 2008 Mar 1;22(1).
- 14 Metz, S. and Trefrey, J.: Chemical and mineralogical influences on concentrations of trace
15 metals in hydrothermal fluids, *Geochim. Cosmo. Acta*, 64, 2267-2279, 2000.
- 16 Middag R, Séférian R, Conway TM, John SG, Bruland KW, de Baar HJ. Intercomparison of
17 dissolved trace elements at the Bermuda Atlantic Time Series station. *Marine Chemistry*.
18 2015 Dec 20;177:476-89.
- 19 Moffett, J. W. and Brand, L. E.: Production of strong, extracellular Cu chelators by marine
20 cyanobacteria in response to Cu stress, *Limnol. Oceanogr.*, 41, 388-395, 1997.
- 21 Moffett, J. W. and Ho, J.: Oxidation of cobalt and manganese in seawater via a common
22 microbially catalyzed pathway, *Geochim. Cosmo. Acta*, 60, 3415-3424, 1996.
- 23 Moore, C. M., Mills, M. M., Achterberg, E. P., Geider, R. J., LaRoche, J., Lucas, M. I.,
24 McDonagh, E. L., Pan, X., Poulton, A. J., Rijkenberg, M. J. A., Suggett, D. J., Ussher, S. J.,
25 and Woodward, E. M. S.: Large-scale distribution of Atlantic nitrogen fixation controlled by
26 iron availability, *Nature Geosci.*, 2, 867-871, 2009.
- 27 Morley, N., Burton, J., Tankere, S., and Martin, J.-M.: Distribution and behaviour of some
28 dissolved trace metals in the western Mediterranean Sea, *Deep Sea Research Part II: Topical*
29 *Studies in Oceanography*, 44, 675-691, 1997.
- 30 Morris, R. M., Vergin, K. L., Cho, J.-C., Rappé, M. S., Carlson, C. A., and Giovannoni, S. J.:
31 Temporal and spatial response of bacterioplankton lineages to annual convective overturn at
32 the Bermuda Atlantic Time-series Study site, *Limnology and Oceanography*, 50, 1687-1696,
33 2005.
- 34 Noble, A. E., Lamborg, C. H., Ohnemus, D., Lam, P. J., Goepfert, T. J., Measures, C. I.,
35 Frame, C. H., Casciotti, K., DiTullio, G. R., Jennings, J., and Saito, M. A.: Basin-scale inputs
36 of cobalt, iron, and manganese from the Benguela-Angola front into the South Atlantic
37 Ocean, *Limnol. Oceanogr.*, 57, 989-1010, 2012.
- 38 Noble, A. E., Saito, M. A., Maiti, K., and Benitez-Nelson, C.: Cobalt, manganese, and iron
39 near the Hawaiian Islands: A potential concentrating mechanism for cobalt within a cyclonic
40 eddy and implications for the hybrid-type trace metals, *Deep Sea Res II*, 55, 1473-1490, 2008.
- 41 Noble, A. E., Saito, M. A., Moran, D. M., and Allen, A.: Dissolved and particulate trace metal
42 micronutrients under the McMurdo Sound seasonal sea ice: basal sea ice communities as a
43 capacitor for iron, *Frontiers in Microbiological Chemistry*, doi: 10.3389/fchem.2013.00025
44 2013.



- 1 Noble AE, Echegoyen-Sanz Y, Boyle EA, Ohnemus DC, Lam PJ, Kayser R, Reuer M, Wu J,
2 Smethie W. Dynamic variability of dissolved Pb and Pb isotope composition from the US
3 North Atlantic GEOTRACES transect. Deep Sea Research Part II: Topical Studies in
4 Oceanography. 2015 Jun 30;116:208-25.
- 5 Ohnemus, D. C. and Lam, P. J.: Cycling of lithogenic marine particles in the US
6 GEOTRACES North Atlantic transect, Deep Sea Research Part II: Topical Studies in
7 Oceanography, 116, 283-302, 2015.
- 8 Olson, R. J., Chisholm, S. W., Zettler, E. R., Altabet, M. A., and Dusenberry, J. A.: Spatial
9 and temporal distribution of prochlorophyte picoplankton in the North Atlantic Ocean, Deep-
10 Sea Research, 37, 1033-1051, 1990.
- 11 Redfield, A. C., Ketchum, B. H., and Richards, F. A. (Eds.): The Influence of Organisms on
12 the Composition of Sea-Water, Wiley, 1963.
- 13 Rodionov, D. A., Vitreschak, A. G., Mironov, A. A., and Gelfand, M. S.: Comparative
14 Genomics of the Vitamin B12 Metabolism and Regulation in Prokaryotes, J. Biol. Chem.,
15 278, 41148-41159, 2003.
- 16 Rue, E. L. and Bruland, K. W.: The role of organic complexation on ambient iron chemistry
17 in the equatorial Pacific Ocean and the response of a mesoscale iron addition experiment,
18 Limnol. Oceanogr., 42, 901-910, 1997.
- 19 Saito, M. A. and Goepfert, T. J.: Zinc-cobalt colimitation in *Phaeocystis antarctica*, Limnol.
20 Oceanogr., 53, 266-275, 2008.
- 21 Saito, M. A., Goepfert, T. J., Noble, A. E., Bertrand, E. M., Sedwick, P. N., and DiTullio, G.
22 R.: A seasonal study of dissolved cobalt in the Ross Sea, Antarctica: micronutrient behavior,
23 absence of scavenging, and relationships with Zn, Cd, and P, Biogeosciences, 7, 4059-4082,
24 2010.
- 25 Saito, M. A. and Moffett, J. W.: Complexation of cobalt by natural organic ligands in the
26 Sargasso Sea as determined by a new high-sensitivity electrochemical cobalt speciation
27 method suitable for open ocean work, Mar. Chem., 75, 49-68, 2001.
- 28 Saito, M. A. and Moffett, J. W.: Temporal and spatial variability of cobalt in the Atlantic
29 Ocean, Geochim. Cosmochim. Acta, 66, 1943-1953, 2002.
- 30 Saito, M. A., Moffett, J. W., and DiTullio, G.: Cobalt and Nickel in the Peru Upwelling
31 Region: a Major Flux of Cobalt Utilized as a Micronutrient, Global Biogeochem. Cycles, 18,
32 doi:10.1029/2003GB002216 2004.
- 33 Saito, M. A., Noble, A. E., Tagliabue, A., Goepfert, T. J., Lamborg, C. H., and Jenkins, W. J.:
34 Slow-spreading submarine ridges in the South Atlantic as a significant oceanic iron source,
35 Nature Geosci, 6, 775-779, 2013.
- 36 Saito, M. A., Rocap, G., and Moffett, J. W.: Production of cobalt binding ligands in a
37 *Synechococcus* feature at the Costa Rica Upwelling Dome, Limnol. Oceanogr., 50, 279-290,
38 2005.
- 39 Schlitzer, R. Ocean Data View, version 4.4.2 [Internet]. Available from <http://odv.awi.de>,
40 2011.
- 41 Scrosati, B. and Garche, J.: Lithium batteries: Status, prospects and future, Journal of Power
42 Sources, 195, 2419-2430, 2010.



- 1 Shelley, R., Sedwick, P. N., Bibby, T., Cabedo-Sanz, P., Church, T., Johnson, R., Macey, A.,
2 Marsey, C., Sholkovitz, E., Ussher, S., and Worsfold, P.: Controls on dissolved cobalt in
3 surface waters of the Sargasso Sea: Comparisons with iron and aluminium, *Global*
4 *Biogeochem. Cycles*, 26, 2012a.
- 5 Shelley, R. U., Morton, P. L., and Landing, W. M.: Elemental ratios and enrichment factors in
6 aerosols from the US-GEOTRACES North Atlantic transects, *Deep Sea Research Part II:*
7 *Topical Studies in Oceanography*, 116, 262-272, 2015.
- 8 Shelley, R. U., Sedwick, P. N., Bibby, T. S., Cabedo-Sanz, P., Church, T. M., Johnson, R. J.,
9 Macey, A. I., Marsay, C. M., Sholkovitz, E. R., Ussher, S. J., Worsfold, P. J., and Lohan, M.
10 C.: Controls on dissolved cobalt in surface waters of the Sargasso Sea: Comparisons with iron
11 and aluminum, *Global Biogeochemical Cycles*, 26, GB2020, 2012b.
- 12 Skogen, M.: A biophysical model applied to the Benguela upwelling system, *South African*
13 *Journal of Marine Science*, 21, 235-249, 1999.
- 14 Steinberg, D. K., Carlson, C. A., Bates, N. R., Johnson, R. J., Michaels, A. F., and Knap, A.
15 H.: Overview of the US JGOFS Bermuda Atlantic Time-series Study (BATS): a decade-scale
16 look at ocean biology and biogeochemistry, *Deep Sea Research Part II: Topical Studies in*
17 *Oceanography*, 48, 1405-1447, 2001.
- 18 Sterner, R. W. and Elser, J. J.: *Ecological Stoichiometry: The Biology of Elements from*
19 *Molecules to the Biosphere*, Princeton University Press, Princeton NJ, 2002.
- 20 Stramma, L., Johnson, G. C., Sprintall, J., and Mohrholz, V.: Expanding Oxygen-Minimum
21 Zones in the Tropical Oceans, *Science*, 320, 655-658, 2008.
- 22 Sunda, W. and Huntsman, S. A.: Cobalt and zinc interreplacement in marine phytoplankton:
23 Biological and geochemical implications, *Limnol. Oceanogr.*, 40, 1404-1417, 1995.
- 24 Swanner, E. D., Planavsky, N. J., Lalonde, S. V., Robbins, L. J., Bekker, A., Rouxel, O. J.,
25 Saito, M. A., Kappler, A., Mojzsis, S. J., and Konhauser, K. O.: Cobalt and marine redox
26 evolution, *Earth and Planetary Science Letters*, 390, 253-263, 2014.
- 27 Taylor, S. R. and McLennan, S. M.: *The Continental Crust: its Composition and Evolution*,
28 Blackwell Scientific Publications, Boston, 1985.
- 29 Thuróczy, C.-E., Boye, M., and Losno, R.: Dissolution of atmospheric cobalt and zinc in
30 seawater, *Biogeosci.*, 2010. 2010.
- 31 Wu, J., Sunda, W., Boyle, E. A., and Karl, D. M.: Phosphate Depletion in the Western North
32 Atlantic Ocean, *Science*, 289, 752-762, 2000.
- 33 Zhang, H., Van den Berg, C. M. G., and Wollast, R.: The Determination of Interactions of
34 Cobalt (II) with Organic Compounds in Seawater using Cathodic Stripping Voltammetry,
35 *Marine Chemistry*, 28, 285-300., 1990.

36

37

38



Figure 1

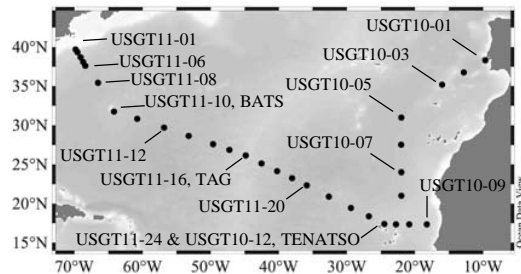




Figure 2

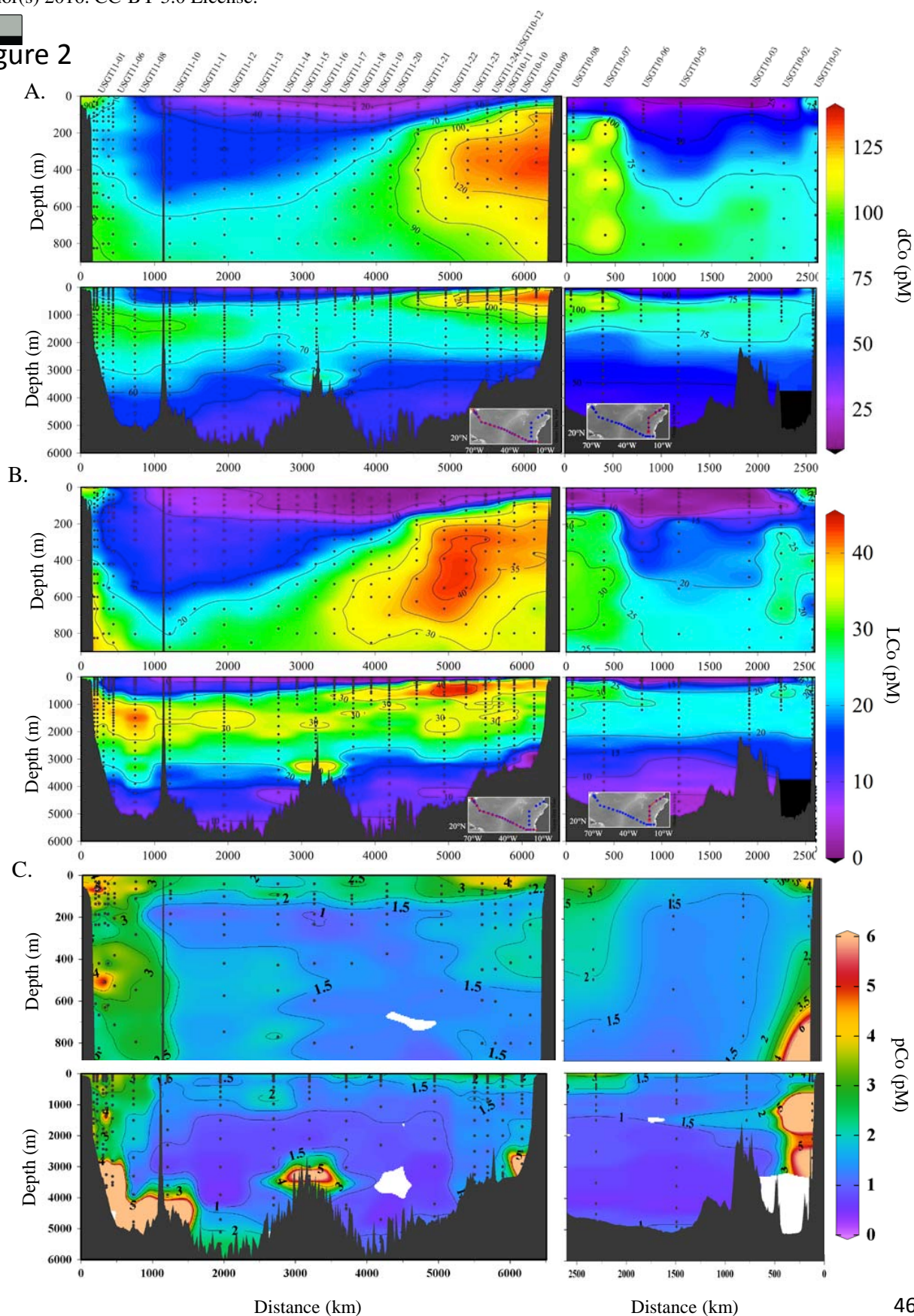




Figure 3

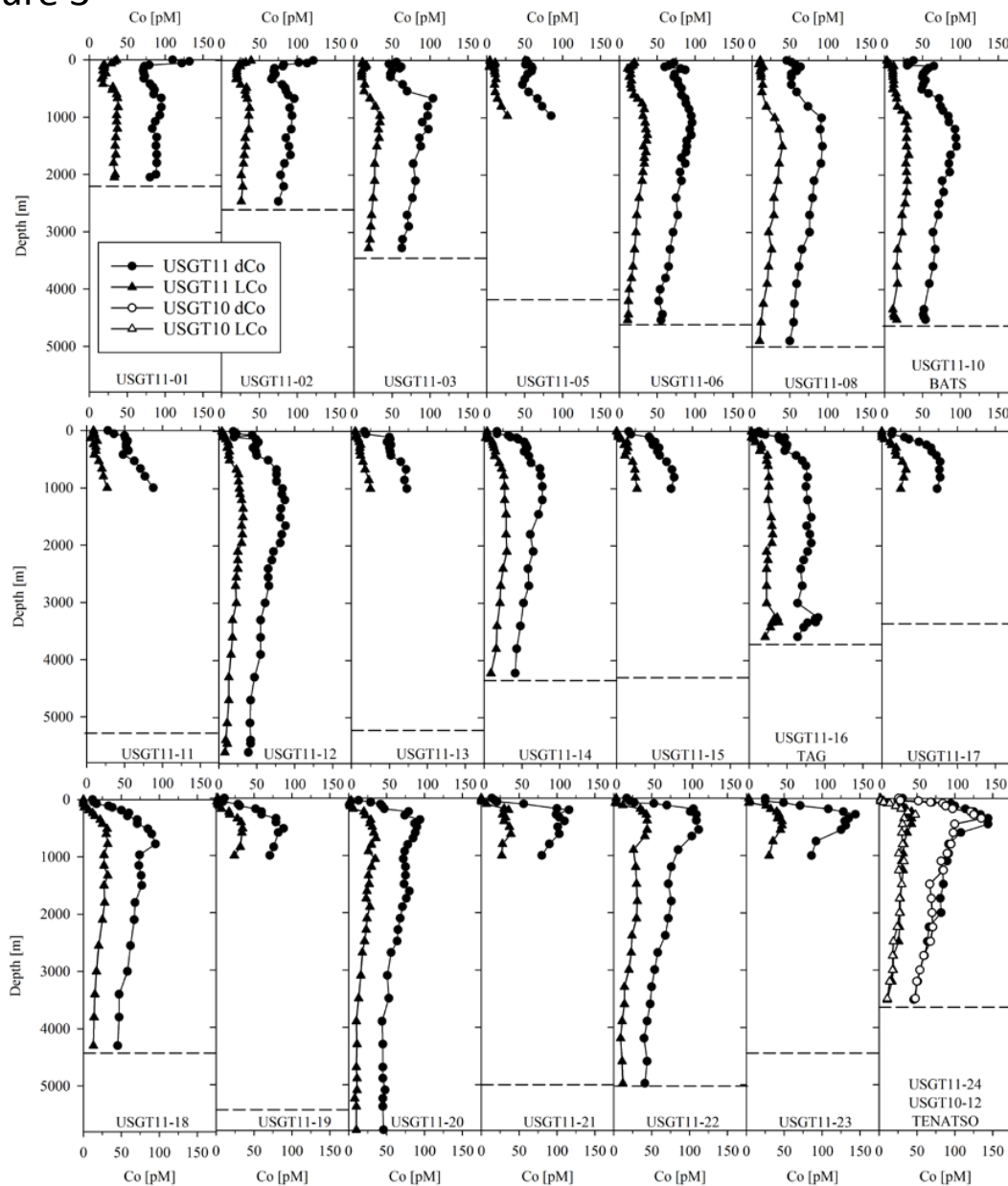




Figure 3

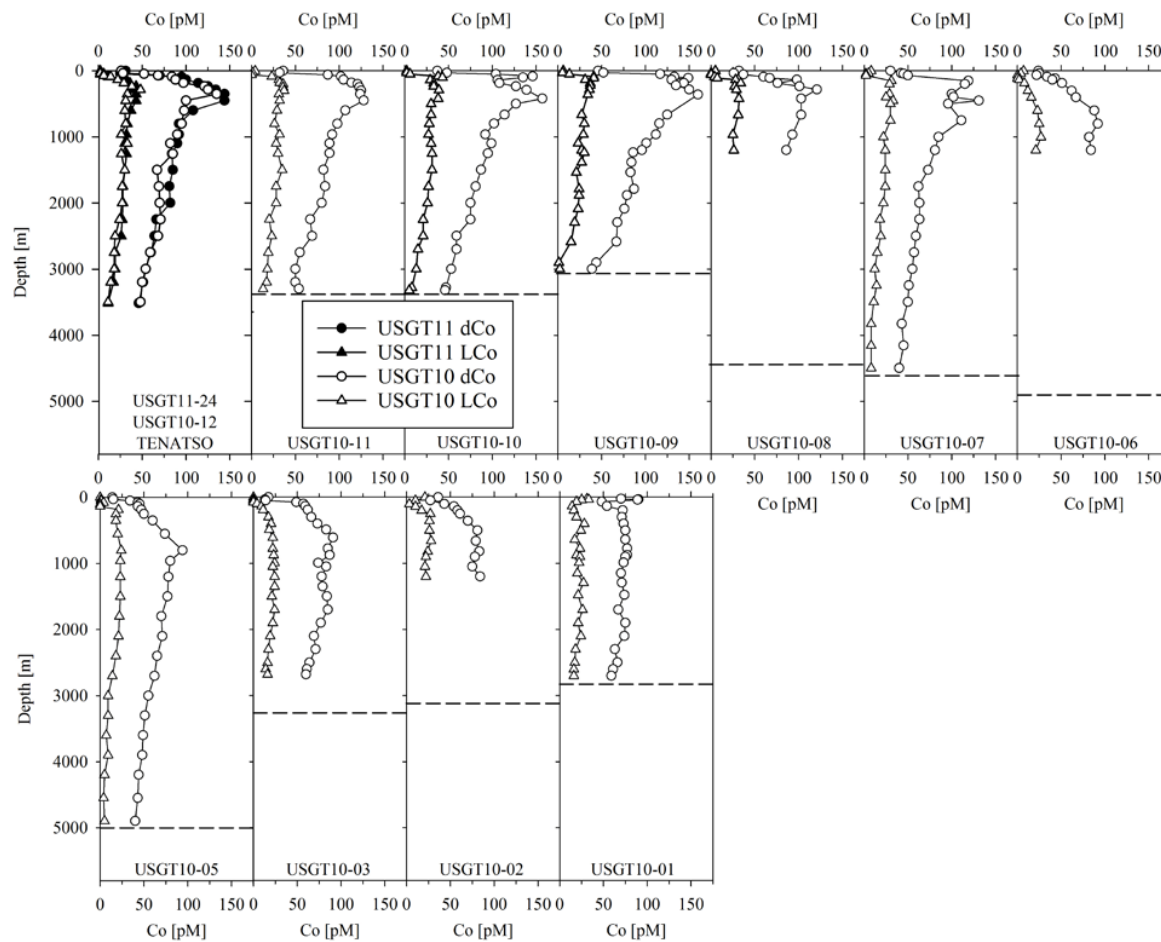




Figure 4

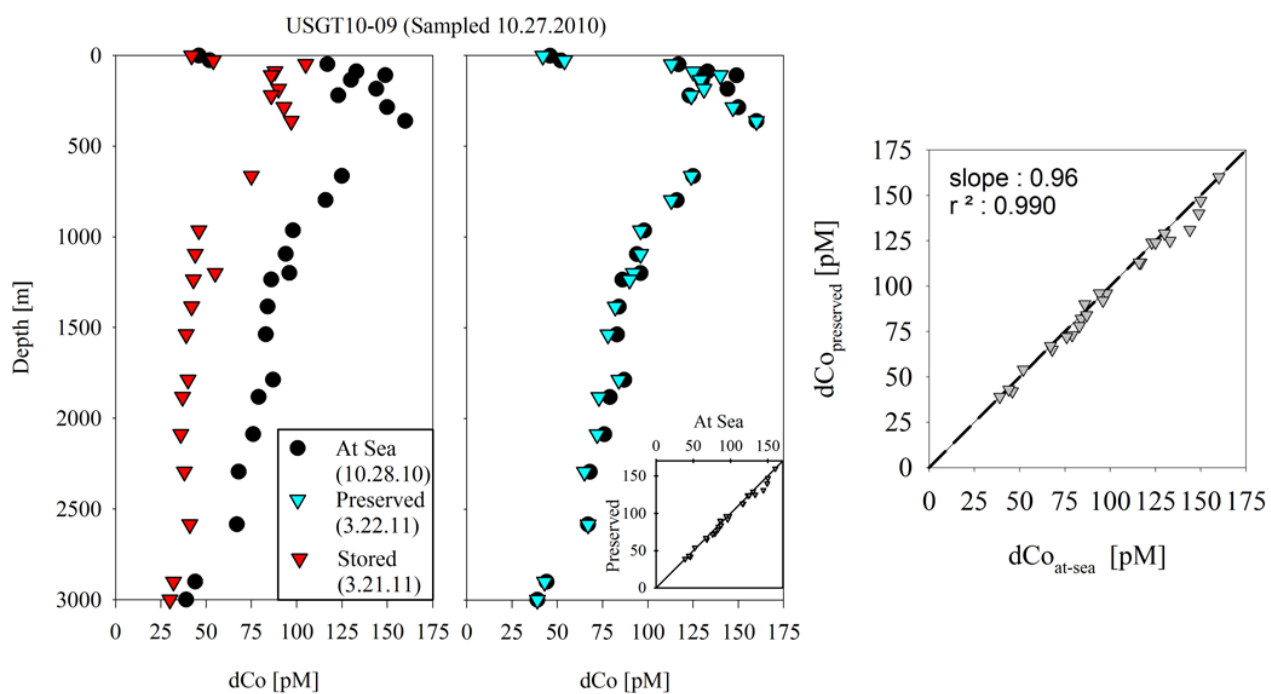




Figure 5

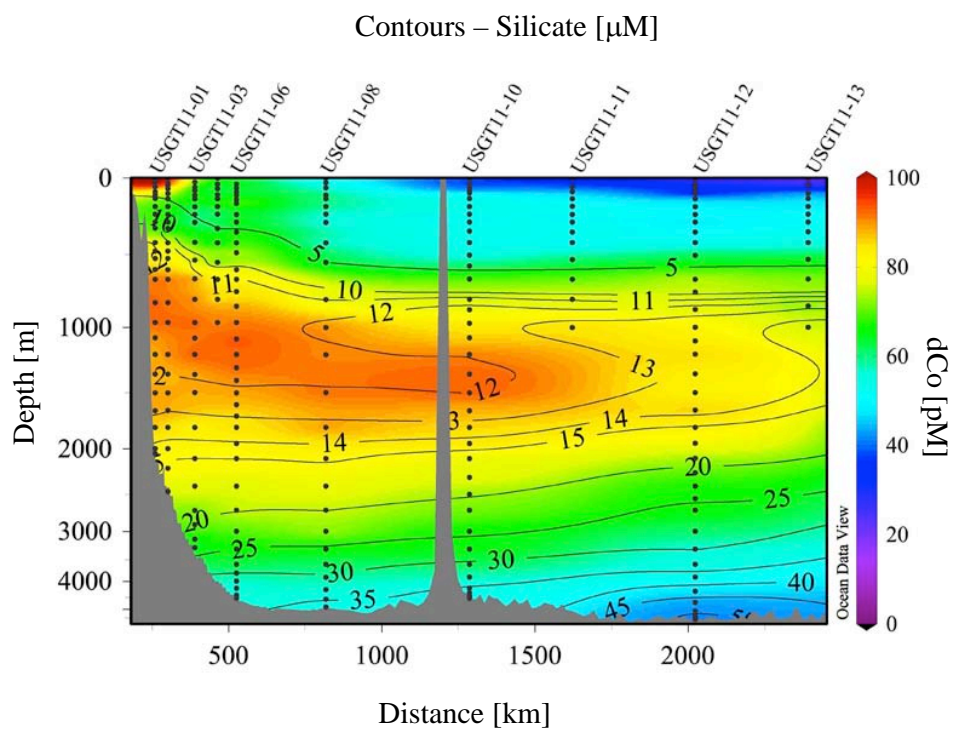




Figure 6

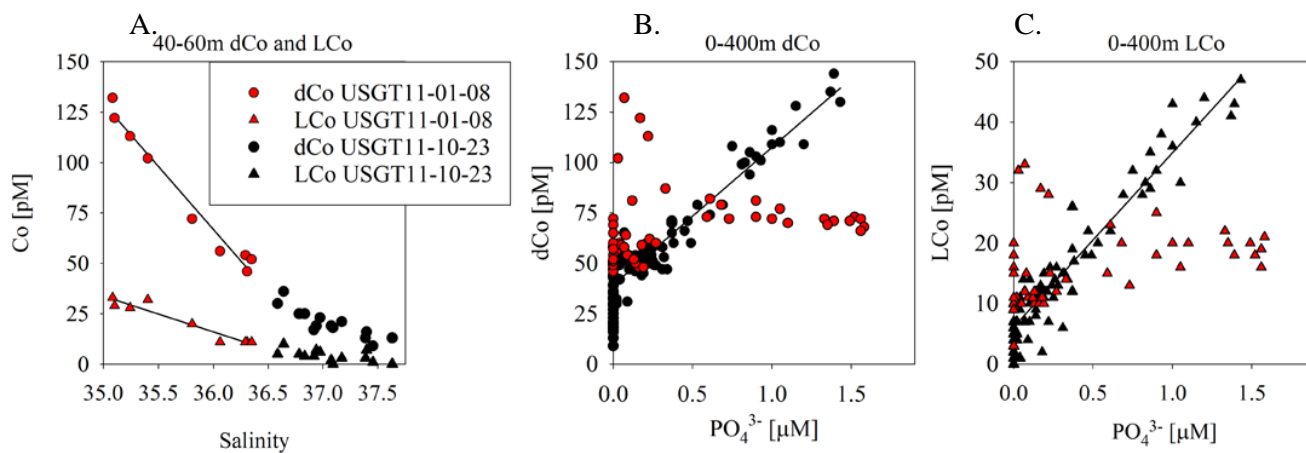




Figure 7

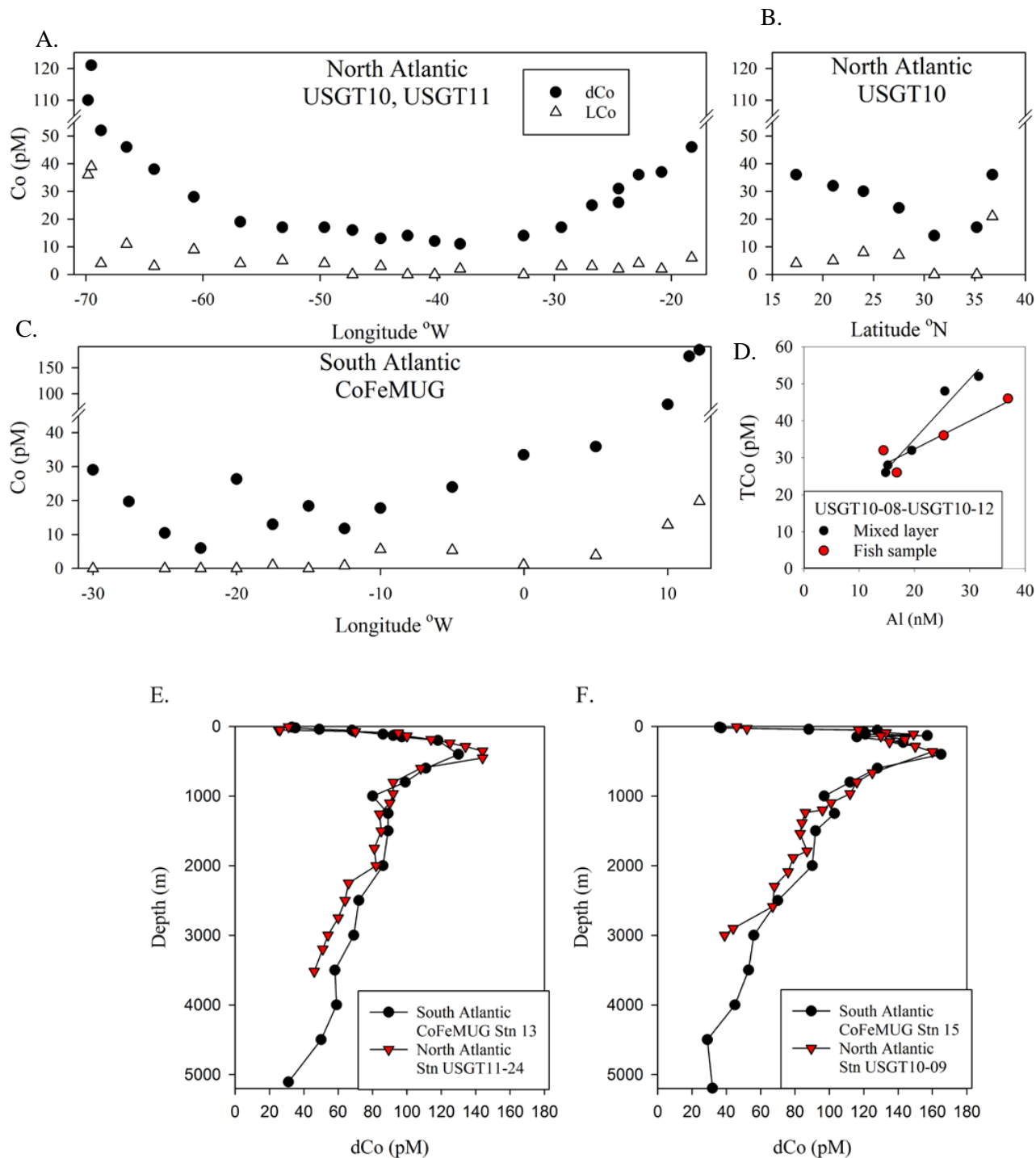




Figure 8

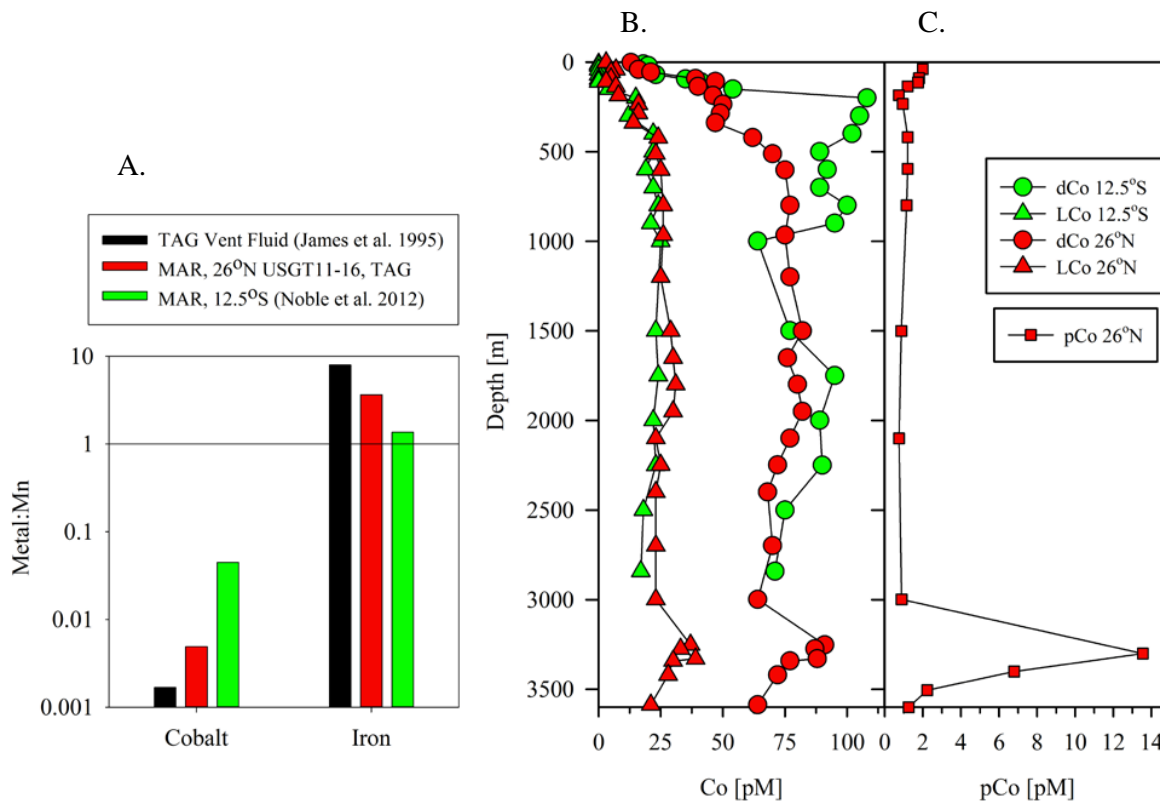




Figure 9

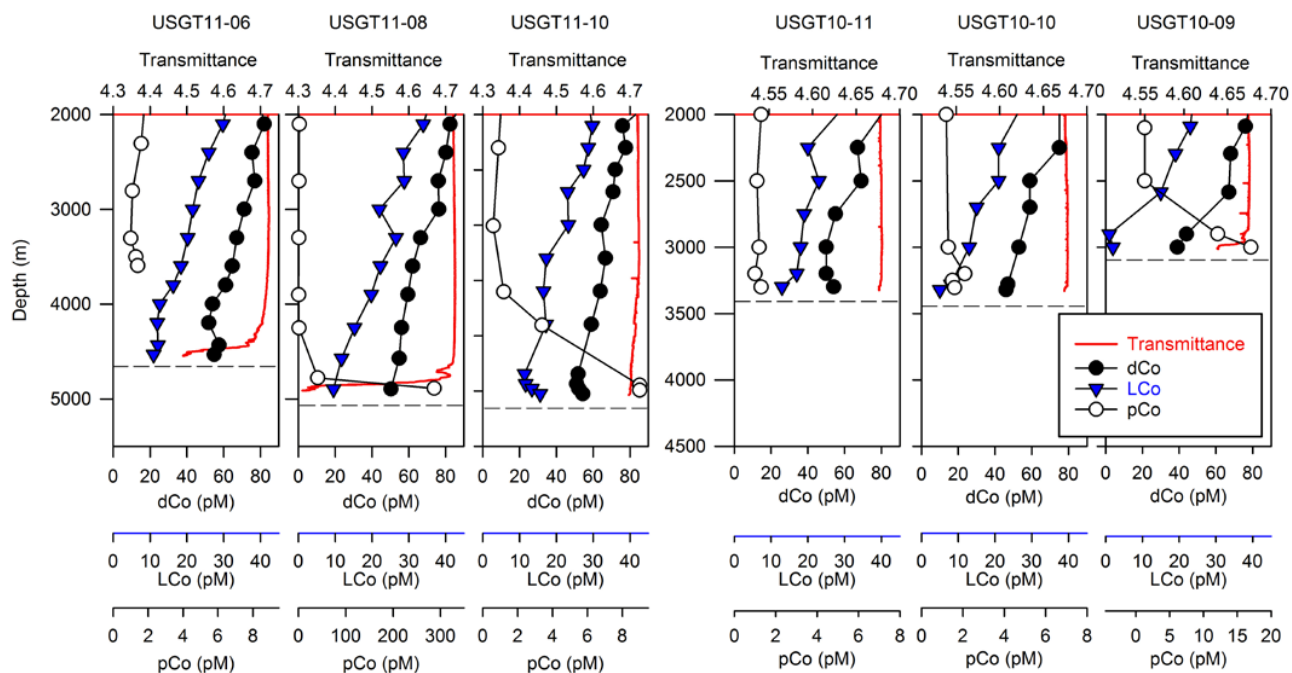




Figure 10

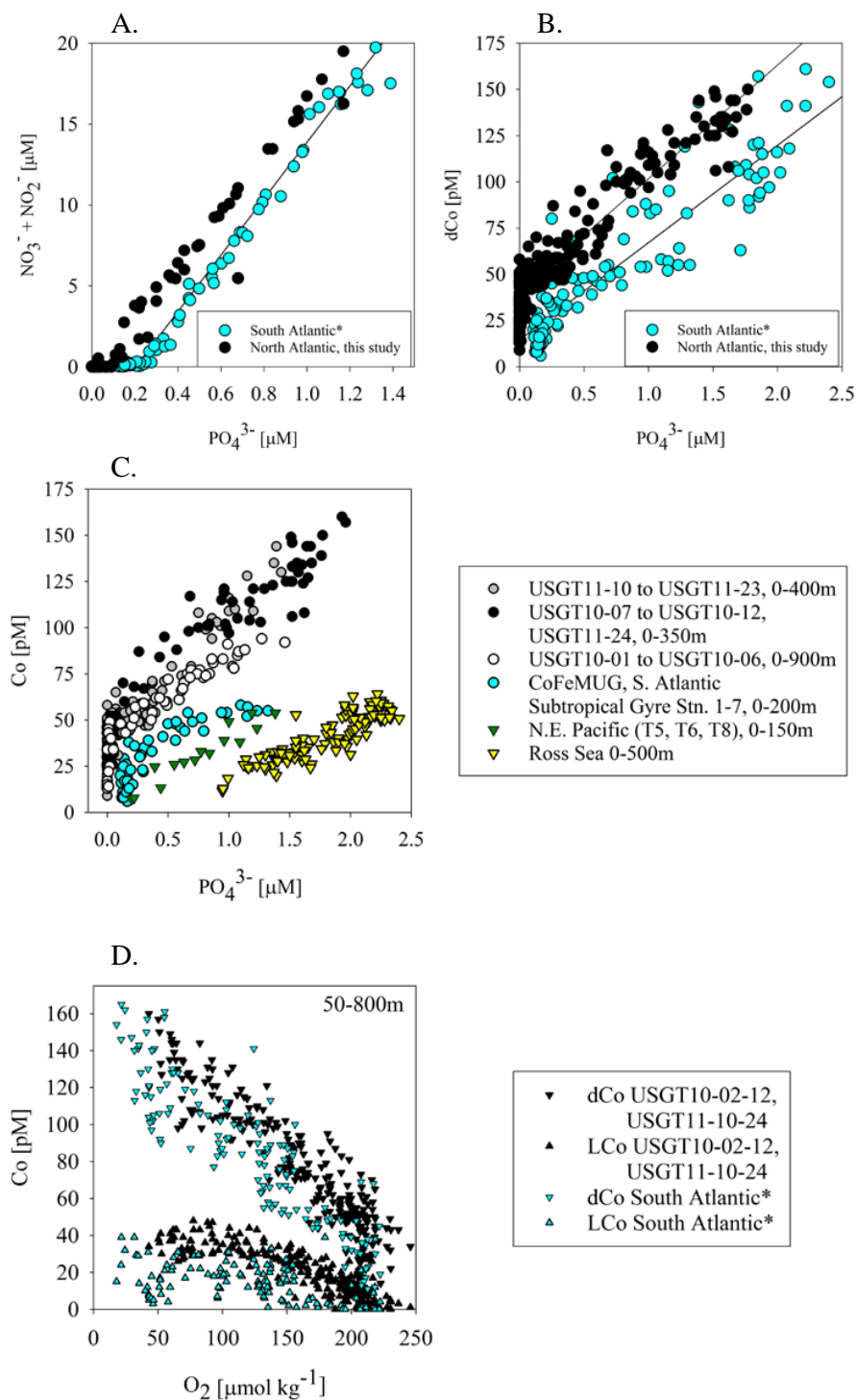




Figure 11

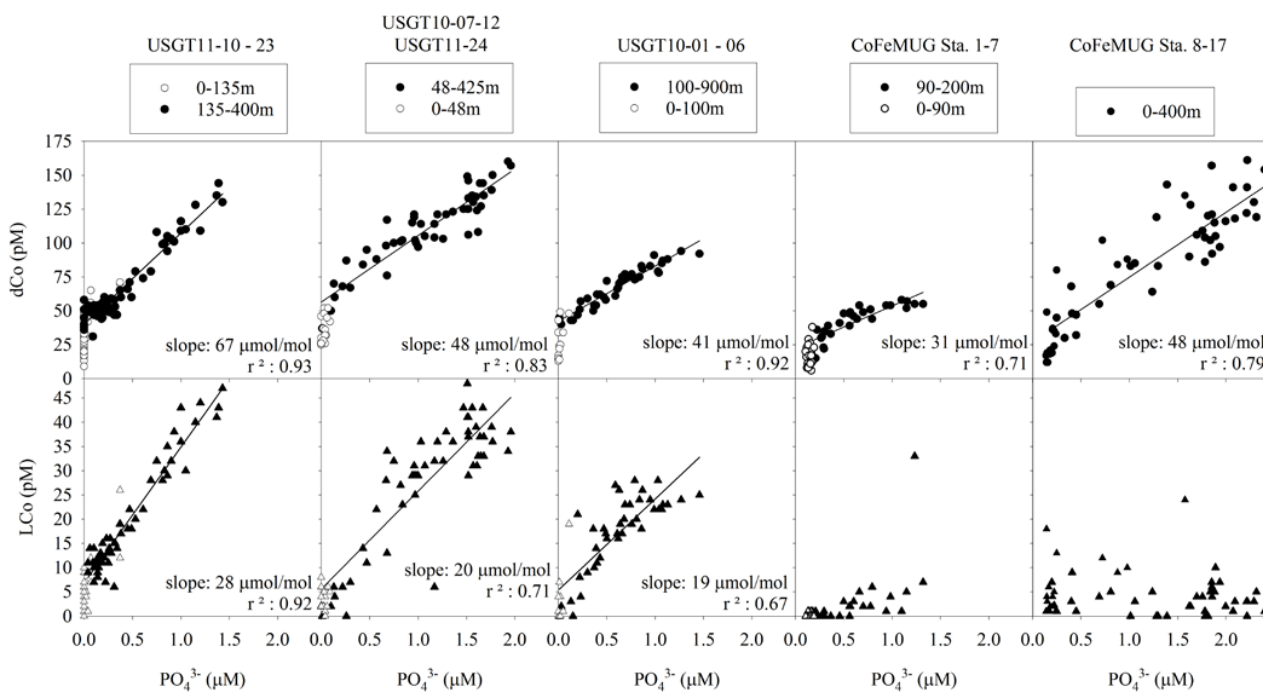




Figure 12

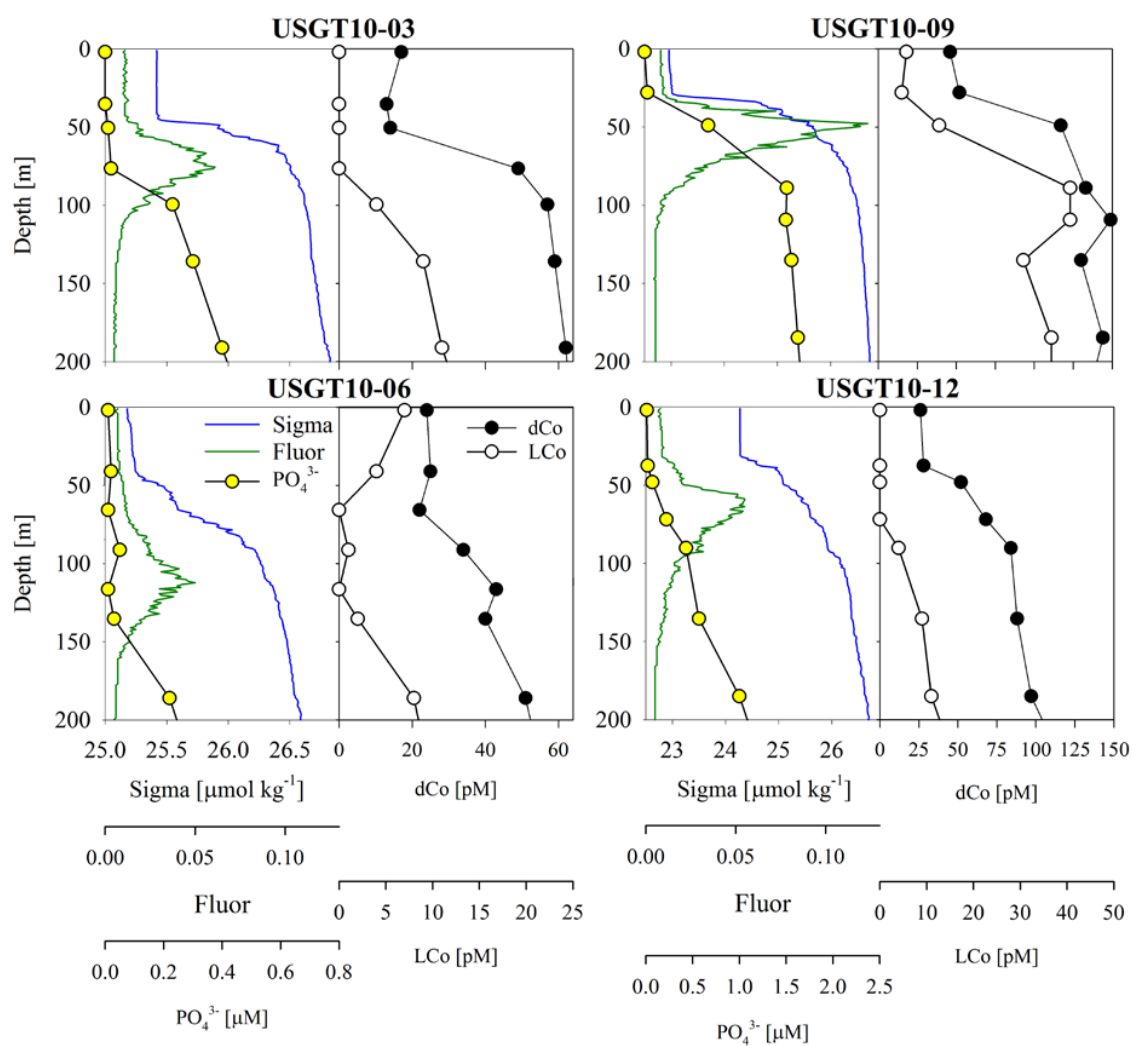




Figure 13

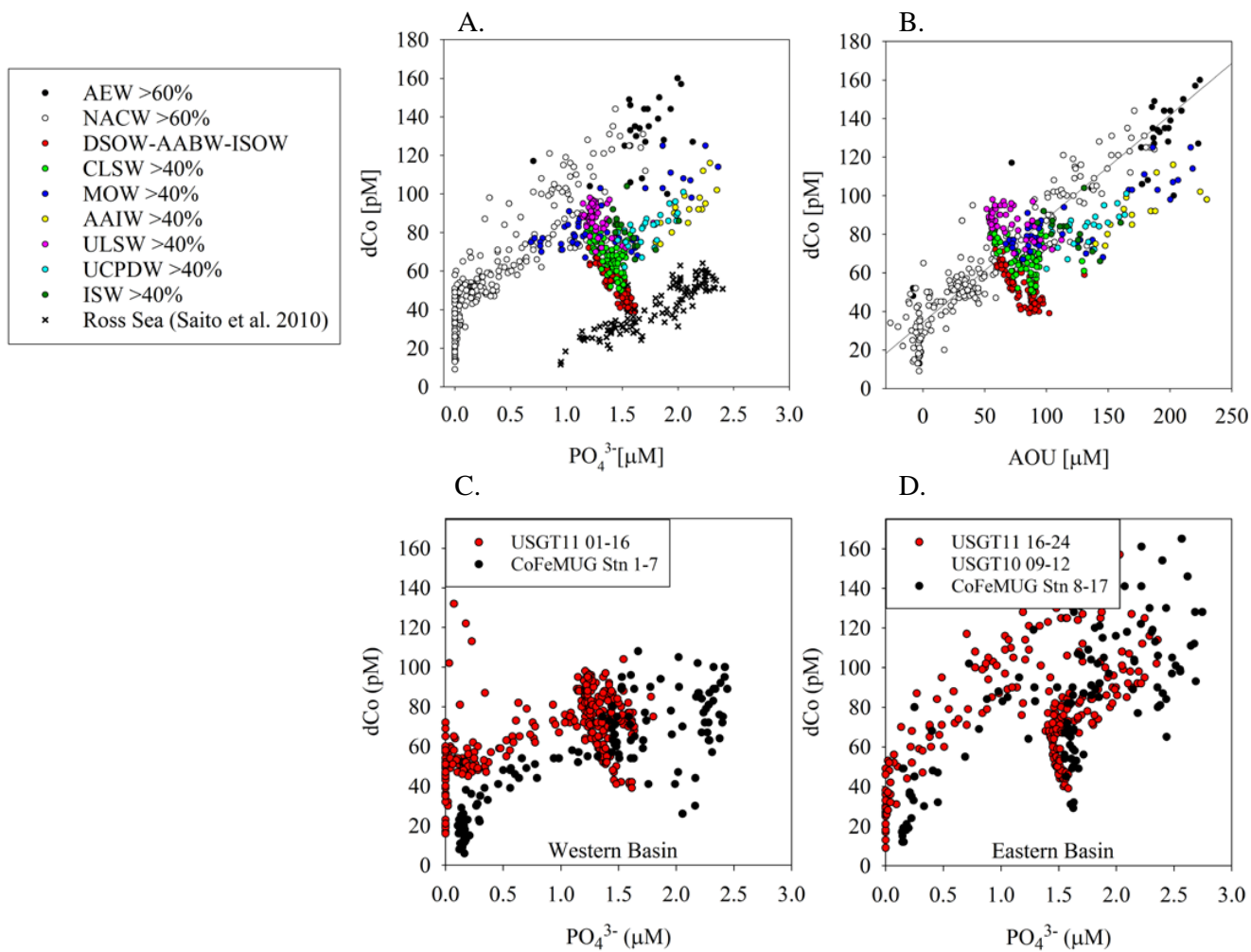




Figure 14

